Results in Engineering 27 (2025) 106735

Contents lists available at ScienceDirect

Results in Engineering

journal homepage: www.sciencedirect.com/journal/results-in-engineering

Research paper

Development of a proof-of-concept concentrating photovoltaic module with integrated tracking and azimuthal cell rotation

Arturo Díaz-Ponce [a,b,*], Iván Trejo-Zúñiga [b], Fernando Dávalos Hernández [c], Pedro M. Rodrigo [c], María A. Ceballos [d], Álvaro Valera-Albacete [d], Florencia Almonacid [d], Eduardo F. Fernández [d,*]

[a] SECIHTI – Centro de Investigaciones en Óptica, A.C., Unidad Aguascalientes, Prol. Constitución 607, Fracc. Reserva Loma Bonita, Aguascalientes, 20200, Aguascalientes, Mexico
[b] Laboratory of Energy Innovation and Intelligent and Sustainable Agriculture (LEIISA), Universidad Tecnológica de San Juan del Río, Av La Palma No 125 Vista Hermosa, San Juan del Río, 76826, Querétaro, Mexico
[c] Universidad Panamericana, Facultad de Ingeniería, Jose María Escrivá de Balaguer 101, Villas Bonaterra, Aguascalientes, 20296, Aguascalientes, Mexico
[d] Advances in Photovoltaic Technology (AdPVTech), CEACTEMA, University of Jaén, Las Lagunillas Campus, Jaén, 23071, Jaén, Spain

ARTICLE INFO

Keywords:
Micro-tracking
Tracking-integrated
CPV
Agrivoltaics

ABSTRACT

Photovoltaics can be more efficient by concentrating the sunlight onto multi-junction solar cells. However, conventional concentrator systems require expensive solar trackers. Recently, the micro-tracking concept, developed inside the photovoltaic module, has emerged as a way to improve competitiveness by eliminating the need for an external tracker. This study presents the design and laboratory validation of a proof-of-concept wide-acceptance-angle tracking integrated micro-concentrator photovoltaic (WiT-CPV) system, featuring a pioneering azimuthal cell rotation mechanism. This innovation ensures perpendicular alignment with incident solar rays in the azimuthal axis, enhancing optical efficiency while reducing mechanical complexity compared to conventional dual-axis tracking systems. The WiT-CPV employs a biconvex aspheric lens and three linear actuators to achieve precise micro-tracking within ±30° zenithal and ±40° azimuthal ranges. Laboratory tests confirm that single-axis azimuthal rotation captures 72–74% of two-axis rotation energy gains, with annual energy improvements of 3.15% (Aguascalientes, Mexico) and 2.87% (Jaen, Spain) over micro-tracking non-rotating systems. The prototype exhibits stable optical efficiency at low incidence angles (0°–25°). Transparent materials enable the transmission of diffuse radiation, supporting agrivoltaic applications. The system's modular design, using cost-effective PMMA lenses and PET brackets, enhances scalability and economic viability. This proof-of-concept study, focused on optical and mechanical performance, did not assess material degradation or outdoor performance. Future work will involve integrating durable materials and conducting field trials to validate long-term performance and the levelized cost of electricity. The WiT-CPV provides a scalable and efficient solution for sustainable solar energy generation, particularly in resource-constrained environments.

1. Introduction

As the global push for renewable energy accelerates, there is an increasing need to improve the efficiency of solar technologies, especially those that concentrate sunlight, such as concentrated photovoltaic (CPV) and concentrated solar power (CSP) systems. CPV has shown great potential, achieving high conversion efficiencies in both research environments and commercial applications [1,2]. However, reaching the full capabilities of these systems involves more than just precise optics and advanced multi-junction solar cells (MJSCs). It also requires solving practical challenges, such as thermal management and spectral optimization, and, most importantly, maintaining accurate solar tracking throughout the day [3,4]. These technologies employ optical components such as Fresnel lenses [5–7], parabolic mirrors [5,8,9], and bi-convex aspheric lenses [10], among others

* Corresponding authors at: SECIHTI – Centro de Investigaciones en Óptica, A.C., Unidad Aguascalientes, Prol. Constitución 607, Fracc. Reserva Loma Bonita, Aguascalientes, 20200, Aguascalientes, Mexico.
E-mail addresses: adiaz@cio.mx (A. Díaz-Ponce), eduardo.fernandez@ujaen.es (E.F. Fernández).

https://doi.org/10.1016/j.rineng.2025.106735
Received 25 June 2025; Received in revised form 8 August 2025; Accepted 12 August 2025

Available online 27 August 2025
2590-1230/Published by Elsevier B.V. This is an open access article under the CC BY-NC-ND license (http://creativecommons.org/licenses/by-nc-nd/4.0/).

Nomenclature

Acronyms

CPV Concentrator photovoltaic
CSP Concentrator solar power
DNI Direct normal irradiance
HCPV High-concentration photovoltaic
LCOE Levelized cost of electricity
MCU Microcontroller unit
MJSC Multi-junction solar cell
PET Polyethylene terephthalate
PMMA Polymethyl methacrylate
POE Primary optical element
PV Photovoltaic
SMA Shape memory alloys
TMY Typical meteorological year
WiT-CPV Wide-acceptance-angle tracking-integrated micro-CPV
BOS Balance of system (non-module components and installation)

Latin Characters

AOI Angle of incidence ..... °
d_k Direction of motor movement ..... –
d_{long} Site longitude ..... °
$\Delta I_{sc,k}$ Increment of I_{sc} at step k ..... A
Δx_{k-1} Displacement from the previous iteration ..... –
E Energy ..... J
EI Energy improvement ..... %
EQE External quantum efficiency ..... –
EIF Energy improvement factor ..... –
E_t Equation of time ..... h
$F(\theta)$ Angular factor ..... –
H_s Solar hour ..... h
I_{sc} Short-circuit current ..... A
k Iteration index ..... –
N Number of iterations ..... –
n Day of year ..... –
P Power ..... W
V_{oc} Open-circuit voltage V
ω Hour angle ..... °
UTC Coordinated universal time ..... h

Greek Characters

α_{max} Maximum solar altitude ..... °
α_{min} Minimum solar altitude ..... °
α_s Solar elevation angle ..... °
β_{opt} Optimal tilt angle ..... °
Γ Fractional year angle ..... °
γ_s Solar azimuth angle ..... °
δ Solar declination ..... °
ϕ Site latitude ..... °

[11], to concentrate sunlight onto a smaller target area. In CPV systems, this concentrated radiation is directed onto high-efficiency multi-junction solar cells [12,13], which significantly increase irradiance levels, reduce the required semiconductor area, and enhance conversion efficiency. Under concentrated light, MJSCs have demonstrated energy conversion efficiencies exceeding 47% [14]. In CSP systems, particularly parabolic trough collectors, solar radiation is concentrated along the linear focal axis of the parabola, where a receiver absorbs the energy [15,16]. This configuration enables working temperatures ranging from 100 °C to 400 °C [17,18], making it suitable for diverse thermal processes such as pasteurization, food preparation, cleaning, distillation, fluid heating, and boiler feedwater preheating [18–22]. In addition to electricity generation, solar energy is also being harnessed for diverse thermal applications: box-type cookers with sensible-heat storage enable evening meal preparation without fossil fuels [23], packed-bed–assisted solar stills deliver potable water during off-sunshine hours [24], and desiccant-assisted ventilation systems regenerated by rooftop collectors cut building cooling electricity by up to 24% in warm-humid climates [25]. In particular, CPV technology has demonstrated strong versatility in space-constrained scenarios, including zero-energy buildings [26], where recent optical reviews highlight micro-tracking systems as a leading approach for maximizing facade-integrated energy yield [27]. Recent developments also emphasize the potential of integrating micro-tracking PV technologies into building facades, where compact and precise alignment mechanisms can maximize solar collection in limited urban spaces [28]. Beyond urban settings, CPV systems are ideally suited for agrivoltaic applications, in which electricity generation and crop cultivation share the same land. Reported land equivalent ratios (LERs) of 1.2 to 1.6 highlight the potential for more efficient land use compared to separate systems [29]. In arid regions, CPV modules not only boost energy production but also provide partial shading, which reduces soil evaporation and mitigates extreme temperatures, factors that can enhance crop yields. By uniting food and energy production, CPV supports sustainable resource use and climate-resilient agriculture. Despite these advantages, the practical implementation of CPV technology faces challenges such as accurate solar alignment, thermal management, and heat dissipation, as well as optical and electrical mismatch losses [30,31]. Mainly, maintaining accurate solar alignment requires high-precision tracking mechanisms, especially under varying weather conditions [1,32]. Traditional tracking systems, which rely on large-scale mechanical structures, increase system complexity and costs, thereby limiting the feasibility of CPV in compact or distributed applications. In high-concentration photovoltaic (HCPV) systems, even minor tracking errors can lead to misalignment, resulting in efficiency losses [33]. While the required tracking precision varies depending on the optical design and application, many CPV systems demand fine angular control to maintain optimal performance. These factors restrict CPV's accessibility for small-scale and residential installations, where space and weight constraints add further limitations [34]. Given these challenges, alternative tracking approaches, such as integrated micro-tracking systems [35], offer a promising and innovative solution. Micro-tracking enables CPV deployment in compact settings by eliminating the need for large-scale mechanical structures and reducing system complexity, weight, and susceptibility to wind loads. Additionally, micro-tracked CPV technology is cost-competitive with photovoltaic (PV) in behind-the-meter applications, particularly in urban environments where land costs are high [36]. Hence, advancing micro-tracking technology is essential for establishing CPV as a scalable and economically viable component of renewable energy infrastructure.

Integrated micro-tracking offers an advantageous alternative to conventional tracking systems. Instead of relying on large external structures, this approach achieves solar alignment by moving optical elements or solar cells internally within the CPV module. This internal motion improves both the precision and efficiency of solar energy capture. By incorporating laterally shifting optics or mobile cells inside a fixed concentrator housing [37–39], the need for bulky external mechanisms is eliminated. As a result, micro-tracking not only complements traditional tracking systems but also expands their applicability to environments where structural constraints make conventional designs impractical. Early micro-tracking implementations replaced traditional two-axis tracking with internal solar cell translations, reducing mechanical stress and maintenance requirements [37]. Another early approach utilized laterally moving optics, where plano-convex lenses or other refractive elements shifted laterally to dynamically

align with sunlight [38,39]. Growing upon these initial findings, modern tracking-integrated CPV systems now fall into three main categories [35]: (1) tracking concentrator elements, (2) external trackers, and (3) internal trackers. These designs can be classified into two types within internal tracking systems: a) mechanically actuated solar cell displacement and b) optical waveguide-based tracking. In particular, mechanically actuated systems use precise movement mechanisms to keep the solar cell at the concentrator's focal point, ensuring optimal alignment and energy conversion. Recent advancements in integrated tracking for CPV modules have introduced planar sliding mechanisms that enable solar cell displacement without rotation, achieving optical efficiencies exceeding 70% and maintaining effective tracking for incidence angles up to 40° [40–43]. Other approaches leverage shape memory alloys (SMA) to actuate the cell, eliminating the need for motors and enabling planar motion without inducing cell rotation [44,45]. While these systems significantly reduce power consumption, they present inherent challenges, including the highly nonlinear behavior of SMA dynamics and its strong dependency on temperature variations, which can compromise tracking accuracy and stability. Additionally, some designs incorporate passive displacement along the Z-axis, enabling three-dimensional tracking and enhancing focal alignment along the Petzval curve [46,44]. However, a fundamental limitation persists: the absence of cell rotation. Since the cell remains flat throughout the tracking process, it does not maintain perpendicularity to the concentrated rays, resulting in an angular mismatch and potential reductions in energy conversion efficiency. A more detailed and extended comparison of micro-tracking methods can be found in Subsection 7.6.

While recent developments have improved certain aspects, existing internal micro-tracking mechanisms in CPV systems continue to face critical limitations in optimizing energy conversion efficiency and angular acceptance while ensuring mechanical robustness and cost-effectiveness. A fundamental constraint arises from the predominantly planar motion of the solar cells or optical elements, which limits alignment capabilities to translational degrees of freedom. Most reported prototypes cannot rotate the solar cell, resulting in suboptimal angular orientation with respect to the incident radiation, particularly along the azimuthal axis. This planar-only displacement results in an angular mismatch between the incoming concentrated rays and the cell surface. Consequently, these systems cannot maintain the perpendicularity of the rays focused on the CPV cell throughout the entire field of view, which is essential for maximizing energy capture. Moreover, most current designs do not account for the curvature of the Petzval surface, a geometric effect that arises due to the focal plane deformation when tracking off-axis solar positions. The inability to dynamically conform to this curved focal surface further limits the optical coupling efficiency, especially at higher incidence angles. These shortcomings underscore the need for innovative micro-tracking solutions that integrate both rotational and translational motion, enabling the solar cell to follow intricate trajectories and maintain optimal optical alignment across its entire tracking range.

The aim of the work is to address CPV tracking challenges by developing a proof-of-concept wide-acceptance-angle tracking-integrated micro-concentrator photovoltaic (WiT-CPV) system that enhances energy capture through an innovative micro-tracking mechanism. The research aimed to develop a functional prototype with azimuthal cell rotation, validated through laboratory construction and optical/mechanical characterization, featuring a simplified mechanical design that utilizes cost-effective materials such as polymethyl methacrylate (PMMA) and polyethylene terephthalate (PET). This study extends existing CPV research by introducing the first micro-tracking prototype with azimuthal rotation, overcoming angular misalignment and system complexity, while leveraging transparent materials to enable agrivoltaic applications and reduce production costs and maintenance needs.

The current work is organized as follows: Section 2 outlines the optical modeling process, focusing on optimizing the primary optical element with the help of ray-tracing simulations. Section 3 discusses the experimental characterization of the CPV cells, detailing the measurement setup and procedures used to assess their angular response. Section 4 analyzes different micro-tracking configurations (none, single, and dual cell rotation) for CPV systems, evaluating their impact on energy harvesting efficiency. Section 5 presents the development of the proposed WiT-CPV system, covering the micro-tracking strategy, mechanical design, and the integration of actuators for precise solar tracking. Section 6 explains the proposed controller board and control algorithm, facilitating automated tracking through real-time adjustments based on measured solar radiation. Section 7 presents the experimental results, which include constructing the WiT-CPV prototype, validating movements for both zenithal and azimuthal tracking, and analyzing energy improvements by comparing various micro-tracking approaches. Finally, Sections 8 and 9 present a discussion of the study's findings and conclusions, highlighting the advantages of the WiT-CPV system and outlining potential areas for future research.

2. Optical modeling: design and simulation

The CPV tracking-integrated system consists of a fixed biconvex aspheric lens and a mobile multi-junction MJSC, as previously described by [10]. This lens type addresses the need to reduce spherical aberrations, enabling higher optical efficiency even under irradiance incidence conditions that deviate from the normal. Due to the variation in the angle of incidence, the concentration point of the radiation becomes distorted, making solar tracking more challenging. To minimize this issue, the aspheric lens should also be biconvex, as suggested by [46]. Additionally, the hexagonal geometry of the lens eliminates edge reflection losses that often occur in circular lenses, facilitating the assembly of multiple lenses within a single module. The MJSC, which serves as the tracking element, must move in two directions, both laterally and vertically, to follow the displacement of the concentrated irradiance focus as the angles of incidence (AOI) increases. Fig. 1 presents a ray-tracing diagram of the tracking-integrated system, illustrating the concentration of solar radiation under normal incidence conditions (Fig. 1(a)) and when $AOI \neq 0$ (Fig. 1(b)), without solar cell rotation. The biconvex aspheric PMMA lens, serving as the system's primary optical element (POE), was initially designed through an optimization process to determine its optimal dimensions [10]. This procedure aims to develop a concentrator system with high optical efficiency and angular tolerance. The optimization was performed using the interactive optimizer in TracePro ray tracing software. The final design achieves a concentration level of 82.5×. A more detailed analysis of this process can be found in [10].

To determine the trajectory formed by the POE focal point during its displacement, a set of experimental measurements and simulations are carried out. These results enable the design of the WiT-CPV system so that the CPV cells accurately follow this trajectory. In this study, the CPV cells were displaced laterally and vertically to maximize the short-circuit current (I_{sc}), and an experimental setup was implemented to replicate the displacement observed in the simulations. Fig. 1(c) only shows the x-axis and the x-axis, the axis involved in normal movement in two directions throughout the day. The y-axis would correspond to seasonal movement, related to the elevation of the sun, and is not taken into account in the Fig. 1(c) shown. From the analysis of the simulations, it can be seen that the vertical coordinate of the cell is given by the z-axis. In the experimental setup, the coordinates are obtained directly from the tracking rails denoted as (x_1', z_1'). When $AOI = 0°$, the position of the cell is defined as $x_1' = 12.5$ mm, $z_1' = -29$ mm. To adjust the experimental coordinates with the simulated ones, a correction is performed on both axes. The position x_1' in the solar simulator corresponds to $x_1 = 0$ mm in the simulations. The subsequent x_1' values for $AOI \neq 0°$ are adjusted with respect to this reference to determine the corrected lateral displacement, x_1. For the vertical coordinate, z_1' is measured from the secondary surface of the lens. In this case, the lens thickness is added to z_1', yielding z_1, the corrected vertical displacement. With this adjustment applied to the experimental data,

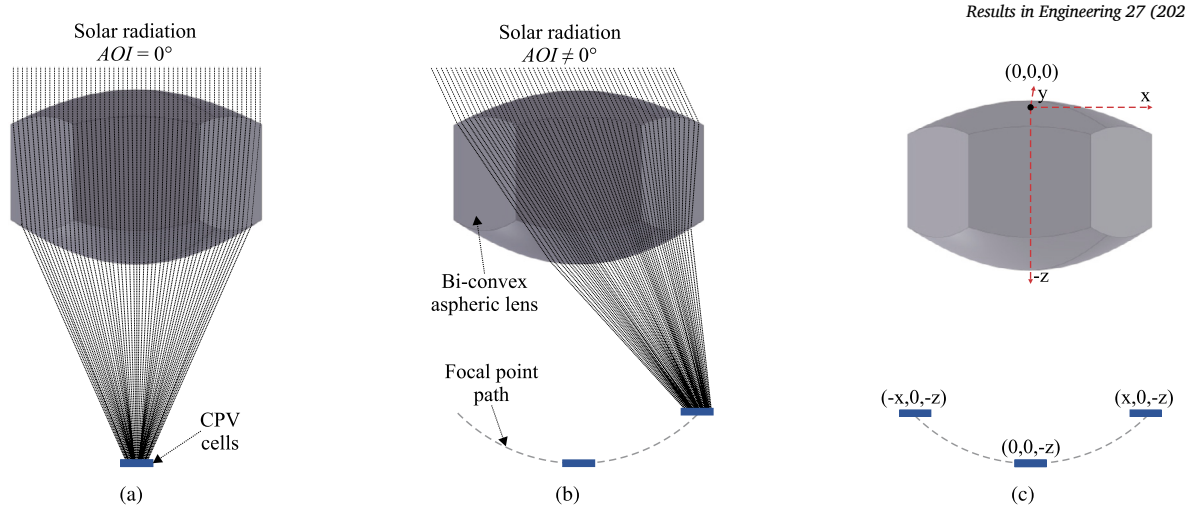


Fig. 1. Schematic of the CPV system ray-tracing: a) solar radiation under normal incidence, b) incident radiation off-axis (without cell rotation), and c) coordinate axis used in the analysis of the trajectory of the focal point of the concentrating lens.

Table 1
Comparison between experimental coordinates (x_1', z_1', x_1, z_1) and simulation coordinates (x_2, z_2) as a function of AOI.

AOI (°)	Experimental coordinates				Simulation coordinates	
	x_1'	z_1'	x_1	z_1	x_2	z_2
0	12.5	-29	0	-72	0	-76
10	22	-28	-9.5	-71	-9.25	-74
20	32	-26	-19.5	-69	-17.5	-71
30	39	-21	-26.5	-64	-25.5	-66.75
40	44.5	-15	-32	-58	-31.75	-61.5
50	48	-9	-35.5	-52	-35.75	-56

the experimental displacement curve can be directly compared with the simulated displacement curve, demonstrating a strong degree of agreement between the two. With this adjustment applied to the experimental data, the displacement curves from both the experimental and simulated cases can be directly compared, demonstrating strong agreement between the experimental results and the simulation, as shown in Table 1.

To obtain analytical approximations of the displacement profile as a function of the angle of incidence ($f_{(x)}$), linear, quadratic, and cubic polynomial regressions were performed using the simulation data to ensure consistency and avoid measurement errors (see Table 1). The resulting models, given by Eqs. (1) (linear), (2) (quadratic), and (3) (cubic), enable accurate modeling of the system's mechanical behavior within the defined range. The mean absolute errors for these approximations were 1.77 mm, 0.53 mm, and 0.18 mm, respectively, with the quadratic model exhibiting the smallest overall error.

$$f_{(x)} \approx 0.537601x_1 - 78.2713, \quad \text{for } 0 \geq x_1 \geq -35.75 \tag{1}$$

$$f_{(x)} \approx 0.015414x_1^2 + 0.0210725x_1 - 75.6712, \quad \text{for } 0 \geq x_1 \geq -35.75 \tag{2}$$

$$f_{(x)} \approx -0.000445291x_1^3 - 0.00834151x_1^2 - 0.285005x_1 - 76.0562, \quad \text{for } 0 \geq x_1 \geq -35.75 \tag{3}$$

The revolved prism defined by Eq. (3) produces a slight peak at the center of the curve. In this study, to simplify the curvature of the displacement profile, the model was constrained to exclude the linear term and the remaining coefficients were reoptimized, resulting in Eq. (4). This constrained model yielded a mean absolute error of 0.46 mm, which was considered acceptable for the system's mechanical design requirements.

$$f_{(x)} \approx -0.000114\,x_1^3 + 0.0108\,x_1^2 - 75.44, \quad \text{for } 0 \geq x_1 \geq -35.75 \tag{4}$$

Once the system's geometry is defined, optical simulations are performed using the TracePro ray-tracing software, which is implemented within the model. The concentration standard test conditions considered include an irradiance of 1000 W/m^2, a temperature of 25 řC, and the AM1.5D reference spectrum. The simulated solar spectrum ranges from 0.3 μm to 2.5 μm, and the angular size of the Sun (4.7 mrad) is also taken into account. The POE uses PMMA, while the MJSC corresponds to a standard triple-junction solar cell composed of gallium indium phosphide (GaInP) as the top subcell, gallium indium arsenide (GaInAs) as the middle subcell, and germanium (Ge) as the bottom subcell. The absorption coefficients of PMMA are taken from [47], and the refractive index values are based on [48], both within the same spectral range previously considered. AZUR SPACE Solar Power GmbH provides the external quantum efficiency (EQE) of the triple-junction solar cell, defined as the ratio of the number of electrons collected at the cell's external contacts to the number of incident photons (Eq. (5)) [49]. This model incorporates both the absorption and angular properties of the CPV system elements, as illustrated in Fig. 2. Table 2 summarizes the key parameters used in the optical simulation of the WiT-CPV system conducted with the TracePro software. Further details on the model and its experimental validation can be found in [50,51].

$$EQE(\lambda) = \frac{\text{number of electrons}}{\text{number of photons}(\lambda)}. \tag{5}$$

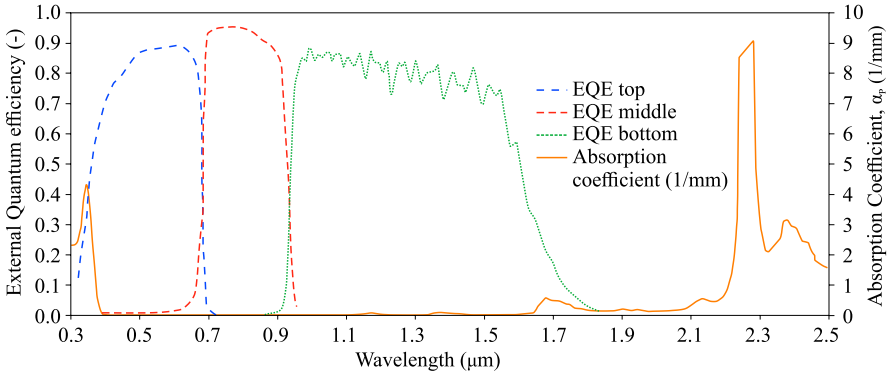


Fig. 2. Optical properties of the system components. External quantum efficiency of each subcell and the absorption coefficient of PMMA.

Table 2
Parameters used in the optical simulation.

Parameter	Value
Solar cell	3C44 – 5,5 × 5,5 mm^2, AZUR SPACE Solar Power GmbH
Solar cell type	Triple-junction GaInP/GaInAs/Ge
Concentration lens type	Biconvex aspheric
Lens material	PMMA
Lens geometry	Hexagonal
Lens dimensions	Diagonal 62 mm, front curvature 0.024 mm^{-1}, rear curvature 0.019 mm^{-1}, thickness 43 mm, and focal length 76 mm [10]
Optical concentration (geometric ratio)	82.5x
Simulated spectral range	0.3 μm – 2.5 μm
Apparent solar angle	4.7 mrad
Concentration standard test conditions	1000 W/m^2, AM1.5D, 25 °C
Refractive index of PMMA	[48]
Absorption coefficient of PMMA	[47]
External quantum efficiency of the cell	[49]

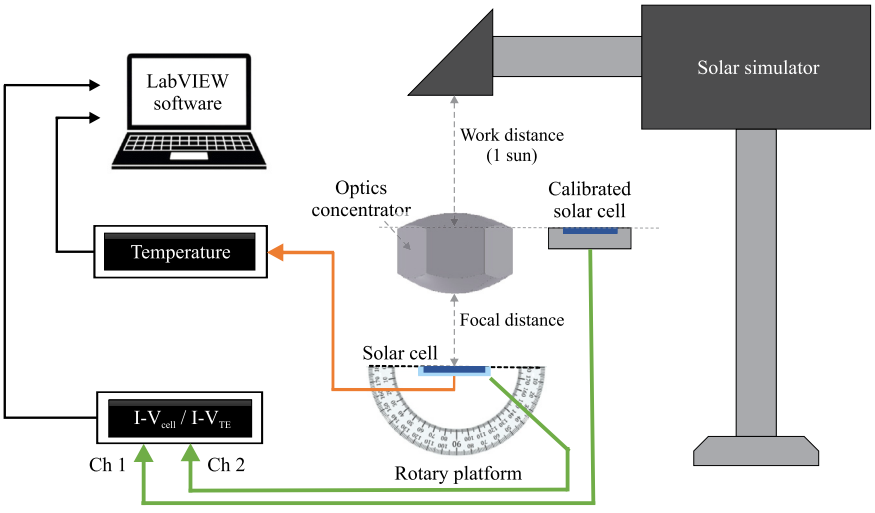
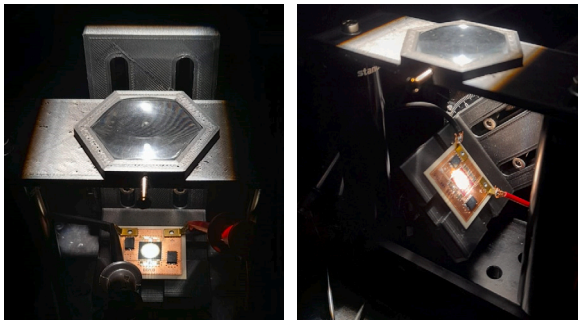


Fig. 3. Scheme of the setup used for the electrical characterization of the solar cell rotated with respect to the concentrated light with a continuous solar simulator.

3. Angular response characterization of CPV cell

To quantify the losses caused in the solar cell by its rotation with respect to the concentrated light, a setup is proposed, whose scheme is shown in Fig. 3. The primary optical lens and solar cell unit were characterized using the Oriel® LCS-100™ small-area solar simulator with an AM1.5 G filter, ensuring compliance with IEC and ASTM standards as per the ABB rating certificate. A standard c-Si reference solar cell (RERA Solution) was employed for irradiance level estimation, meeting the requirements of the IEC 904-2 standard. Current and voltage measurements were extracted using a Keysight Technologies® B2900B™ series source measurement unit, while an Agilent® 34970A data acquisition unit was used for temperature monitoring. Data collection and monitoring were carried out on a laptop using custom LabVIEW® software. A Type J thermocouple was attached to the front of the solar cell before each measurement to ensure the cell temperature remained around 25 °C. Ambient room temperature was maintained at 25 ± 0.5 °C.

The procedure for the measurements consisted of placing the primary lens at a working distance where an irradiance level of 1 sun was ensured. Subsequently, the solar cell's relative distance to the lens's focal point was adjusted by monitoring the I_{sc} until the maximum value was observed.



(a) (b)

Fig. 4. Photographs of the set-up used to measure the solar cell angular response: a) under normal incidence, and b) under inclined incidence.

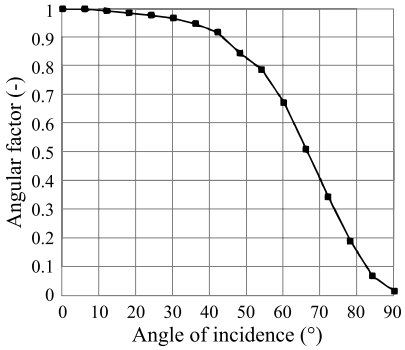


Fig. 5. Measured solar cell angular response (angular factor versus angle-of-incidence) used to characterize the reflective losses on the solar cell surface.

Table 3
Measurement instruments and associated uncertainties.

Instrument	Measurement	Uncertainty
Digital thermometer	Room temperature	±2%
Type-J thermocouple + DAQ AGILENT 34970A	Surface temperature	±1.6%
High precision source/Measure unit B2902B Series	Voltage	±0.4%
High precision source/Measure unit B2902B Series	Current	±0.4%
Error propagation formula	Power*	±0.8%
Error propagation formula	Optical efficiency*	±0.8%
Reference mono-Si solar cell sensor	Irradiance	±3.5%
Total error propagation		±4.52%

* Combined uncertainty.

The solar cell was mounted on the rotation axis of a rotating platform, allowing it to be rotated with respect to the primary lens within a range of angles of incidence (AOI) from 0° to 90°. The I-V characteristic curves at each AOI were measured under the IEC 61215 standard conditions, with an irradiance intensity of 1000 W/m^2, a light spectrum of air mass 1.5G, and a cell temperature of 25 °C. The solar cell's maximum power was extracted from the measured I-V curves for each AOI, and the angular factor (i.e., the ratio of measured maximum power to maximum power under 0° AOI) was calculated. This angular factor decreases as the AOI increases, mainly due to reflective losses. Photographs of the setup under $AOIs$ of 0° and 45° are provided in Fig. 4(a) and 4(b), respectively. The measured angular response (angular factor versus AOI) is presented in Fig. 5.

An uncertainty analysis has been conducted in accordance with the ISO/TR 21900:2018 guide [52]. Estimating the uncertainty in the characterization of photovoltaic systems in a continuous-type solar simulator involves analyzing some factors, which can be sources of uncertainty, including: (1) variations in irradiance from the continuous solar simulator; (2) inaccuracies in current and voltage sensors; and (3) thermal instability in the photovoltaic device under test, among others. The Type A uncertainties were evaluated through statistical analysis, using a minimum of three measures. In contrast, the Type B uncertainties were obtained from the resolution of the measuring instruments or, if available, from the calibrated certificate. Repeatability of measurement indicates the "noise" in the system and should be considered when estimating uncertainty. This also helps to detect possible uncontrolled variations in irradiance or temperature. The combined uncertainties and uncertainty of indirect measurements were assessed using error propagation formulas based on partial derivatives. Expanded uncertainty was calculated with a coverage factor of $k = 2$ (95.45% confidence interval). The values of the estimated uncertainties are presented in Table 3. For determining solar simulator irradiance, the uncertainty for I_{sc} is ±1.7% according to the calibration certificate of the reference solar cell. Combining this error with the repeatability uncertainty associated with the electric current measurements (0.4%) and applying the corresponding coverage factor ($k = 2$), the expanded irradiance uncertainty obtained is ±3.5%. Taking 1,000 W/m^2 as a reference, this variation is equivalent to ±35 W/m^2. Regarding repeatability, a minimum of three measurements of the I-V curves were made and this uncertainty (type A) in combination with the precision of the Keysigth B2920B (type B), a combined uncertainty of 0.4% is obtained (which is what is indicated in Table 3).

Table 3 summarizes the uncertainties associated with the main measurement instruments used during the experimental characterization, including temperature sensors, voltage and current meters, and the reference solar cell. Electrical measurements, performed using a high-precision

Table 4
Experimental parameters and measurement conditions used in the angular response characterization of CPV cell.

Experimental parameter	Measured/used value
Solar simulator	Oriel® LCS-100™, AM1.5G filter
Reference irradiance sensor	Standard c-Si solar cell (RERA Solution)
Standard measurement conditions	IEC 61215 (1000 W/m^2, AM1.5G, 25 °C)
Electrical measurement unit (current–voltage)	Keysight Technologies® B2900B™
Data acquisition unit (temperature)	Agilent® 34970A
Monitoring software	LabVIEW®
Cell temperature measurement	Type J thermocouple, cell surface: 25 ± 0.5 °C
Laboratory ambient temperature	25 ± 0.5 °C
Characterized angular range	0°–90°
Combined uncertainty of the system	Approximately ± 4.52%

source/measure unit (Keysight B2902B), yielded uncertainties of ±0.4% for both current and voltage. These low values reflect the stability and accuracy of the electrical characterization setup. Temperature control, achieved via a Type J thermocouple and data acquisition system, maintained the cell surface temperature at 25 ± 0.5 °C. Considering the relative temperature coefficients provided by the manufacturer (−0.21%/°C for V_{oc} and 0.012%/°C for I_{sc}), a maximum change of 1 °C would imply a drop in V_{oc} of approximately 0.21% and an increase in I_{sc} of less than 0.02%. Since the expected changes in V_{oc} and I_{sc} are below 0.2%, it is assumed that the impact of these temperature fluctuations during the indoor measurements is negligible for the overall system uncertainty. The combined uncertainty in calculated power and optical efficiency, derived through propagation of error, was estimated at ±0.8%, which is acceptable for proof-of-concept validation. Among these parameters, the irradiance sensor exhibits the highest uncertainty, with an expanded value of ±3.5%. However, this does not impact the calculation of optical efficiency, since this parameter is defined as the ratio of the I_{sc} measured under concentration to that measured without the concentrator, using the same solar cell under identical irradiance conditions. Both current measurements (with and without the concentrator) were performed using the same high-precision source/measure unit. Consequently, the expanded uncertainty of the optical efficiency, derived from error propagation, is around ±0.8%, and is independent of the irradiance sensor uncertainty. This distinction is critical, as it clarifies that the most significant source of uncertainty in the setup—irradiance estimation—does not propagate into the optical efficiency calculation. In contrast, it does affect the determination of absolute performance metrics such as electrical efficiency and power output, where irradiance directly enters the denominator of the efficiency equation. Overall, the uncertainty analysis confirms that the reported optical efficiency values are reliable and robust. While irradiance uncertainty is a limiting factor for other performance metrics, it does not compromise the evaluation of optical efficiency or the comparative assessment between tracking configurations. The combined uncertainty for the system, approximately ±4.52%, reflects the cumulative effect of uncertainties from all devices/parameters listed in Table 3, calculated through error propagation. Table 4 summarizes the experimental setup and measurement conditions used for the angular response characterization of the triple-junction solar cell.

4. Evaluation of micro-tracking configurations for CPV systems

The main innovation of the prototype developed in this study is the azimuthal rotation of the solar cell. With this rotation, the angle of incidence of the concentrated light relative to the solar cell surface (θ) can be reduced throughout the day, thereby decreasing reflective losses. The angular response of the solar cell was characterized through the angular factor, $F(\theta)$, with the experimental set-up described in Section 3 (see also Fig. 5). However, a simulation study is required to assess the performance gains achievable by the azimuthal rotation of the solar cell. The basic formulas used for the simulation study are summarized below. In these formulas, we use the 0, 1, and 2 superscripts to refer to three concepts of microtracking configurations:

- 0: No rotation of the solar cell. The cell is held parallel to the concentrating lenses.
- 1: Rotation along a single axis, tracking the azimuthal movement of the sun from east at sunrise to west at sunset.
- 2: Full rotation of the solar cell to achieve normal incidence at every instant. Rotation in the azimuthal and zenith axes.

All concepts (0, 1, and 2) are assumed to be mounted facing the equator and tilted at an angle equal to the latitude. Under this configuration, the angle of incidence (θ) for each device can be expressed as [53]:

$$\theta^0 = \cos^{-1}\left(\sin\alpha_s \cdot \cos\phi + \cos\alpha_s \cdot \sin\phi \cdot \cos\gamma_s\right), \tag{6}$$

$$\theta^1 = |\delta|, \tag{7}$$

$$\theta^2 = 0, \tag{8}$$

where α_s and γ_s are the sun height and azimuth, respectively (with γ_s defined from south to west), ϕ is the latitude, and δ is the solar declination. Given the sun's position and the day of the year, the corresponding θ^j angle of incidence can be calculated for $j = 0, 1$.

The energy improvement factor (EIF) over a specific period for concepts 1 or 2 (relative to device 0) can be defined by Eq. (9), where *DNI* represents the direct normal irradiance, *AOI* is the angle-of-incidence of sunrays relative to the PV module surface, η_{opt} is the optical efficiency as a function of *AOI*, and the subscript "i" denotes a generic interval within the considered period. The optical efficiency function, η_{opt}, was experimentally characterized indoors in a previous study, considering reflection, absorption, non-focusing, and spectral losses [10]. The results of this characterization are presented in Fig. 6. Due to mechanical constraints of the prototype, η_{opt} was truncated for $AOI > 50°$. It is important to mention that the EIF derivation assumes identical spectral effects, thermal behavior, and negligible tracking errors in both rotating and non-rotating microtracking systems. These assumptions simplify the calculation, as a detailed assessment of spectral, thermal, and tracking effects is beyond the scope of this study.

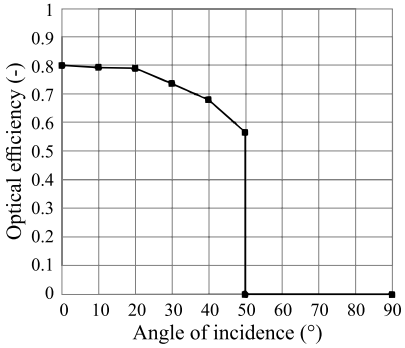


Fig. 6. Optical efficiency as characterized in [10].

$$\mathrm{EIF}^j = \frac{\sum_i \mathrm{DNI}_i \cdot \cos(\mathrm{AOI}_i) \cdot \eta_{\mathrm{opt}}(\mathrm{AOI}_i) \cdot F\left(\theta_i^j\right)}{\sum_i \mathrm{DNI}_i \cdot \cos(\mathrm{AOI}_i) \cdot \eta_{\mathrm{opt}}(\mathrm{AOI}_i) \cdot F\left(\theta_i^0\right)}, \quad j = 1,2 \tag{9}$$

By definition, the EIF quantifies the energy improvement of prototypes 1 or 2 relative to prototype 0 over a specified period, expressed by Eq. (10), where E^j represents the energy harvested by the j-prototype over the considered period, and E^0 is the reference energy harvested by the prototype that does not rotate the solar cell. An $EIF > 1$ indicates energy improvements compared to the reference prototype. Another way to express the same concept is through the percentage energy improvement, $EI(\%)$, which is simply $EI(\%) = (EIF - 1) \cdot 100$, and has positive values when there are energy improvements compared to the reference prototype. This equation enables the evaluation of the energy production achieved by the mechanism proposed in this study. The results are presented in Section 7.5.

$$\mathrm{EIF}^j \approx \frac{E^j}{E^0}, \quad j = 1,2 \tag{10}$$

On the other hand, the apparent sun's position (α_s and γ_s angles) was calculated from the day of the year (n from 1 to 365) and the solar hour (H_s) by the following procedure [54]. First, the solar declination for a specific day of the year is obtained by Eq. (11),

$$\delta = 23.45° \cdot \sin\left(\frac{2\pi \cdot (n + 284)}{365}\right), \tag{11}$$

and the hour angle (ω) for a specific solar hour is obtained as:

$$\omega = -180° + 15°/\mathrm{h} \cdot H_s. \tag{12}$$

From these magnitudes, the sun height and azimuth can be calculated by Eqs. (13) and (14),

$$\alpha_s = \arcsin(\sin\delta \cdot \sin\phi + \cos\delta \cdot \cos\phi \cdot \cos\omega), \tag{13}$$

$$|\gamma_s| = \arccos\left(\frac{\sin\alpha_s \cdot \sin\phi - \sin\delta}{\cos\alpha_s \cdot \cos\phi}\right). \tag{14}$$

It is worth mentioning that typical meteorological year files provide hourly weather data as a function of the Universal Time Coordinated (UTC). Therefore, the H_s must be derived from the UTC by means of the following expression:

$$H_s = \mathrm{UTC} + \frac{\mathrm{long}}{15°/\mathrm{h}} + E_t, \tag{15}$$

where long is the site longitude and E_t is the equation of time, which can be calculated from the day of the year as:

$$E_t = 3.82\,\mathrm{h} \cdot (0.000075 + 0.001868 \cdot \cos\Gamma - 0.032077 \cdot \sin\Gamma - 0.01461 \cdot \cos 2\Gamma - 0.04089 \cdot \sin 2\Gamma) \tag{16}$$

where,

$$\Gamma = \frac{2\pi \cdot (n-1)}{365}. \tag{17}$$

5. Development of the WiT-CPV

5.1. Micro-tracking strategy

Evaluating the solar trajectory for any location and date throughout the year is crucial for designing an effective solar micro-tracking strategy. This evaluation aims to optimize energy generation while reducing the system's energy consumption. Furthermore, the strategy should emphasize the use of low-cost, low-maintenance mechanisms that are relatively easy to construct.

Fig. 7 illustrates the typical apparent path of the Sun as observed from the Earth's surface, extending approximately from east to west throughout the day. Due to this extensive trajectory, the lens's focal point exhibits significant movement along the azimuth axis. Consequently, the CPV cell must track this path and rotate to remain perpendicular to the Sun's rays, ensuring optimal energy capture. This adjustment helps to prevent energy production losses caused by the angle of incidence of solar rays. On the zenithal axis, the solar altitudes exhibit maximum and minimum values. The maximum solar altitude (α_{max}) and the minimum solar altitude (α_{min}) can be determined using Eqs. (18) and (19), respectively [53]. In these equations, ϕ represents the latitude of the location in degrees and δ_{max} corresponds to the maximum solar declination. As shown in Fig. 7, during the

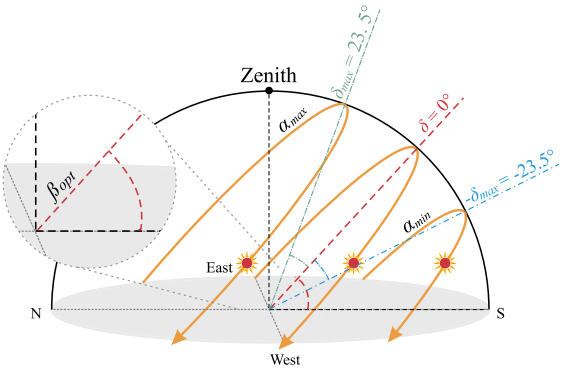


Fig. 7. Typical solar paths for a fixed horizontal observer in the Northern hemisphere.

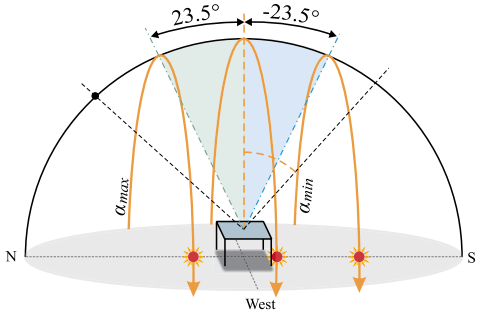


Fig. 8. Typical solar paths for a fixed tilt observer in the Northern hemisphere.

summer solstice, the sun reaches its highest position in the sky, corresponding to a declination angle of $\delta_{max} = 23.5°$. This results in the maximum solar altitude at a given location, α_{max}. Conversely, the Sun reaches its maximum negative declination at the winter solstice, $-\delta_{max} = -23.5°$, resulting in the minimum solar altitude, α_{min}. Therefore, to ensure that the CPV cell can reach all potential positions of the focal point generated by the concentrating lens—regardless of location and date—it is practically necessary that the microtracking system can move the cells in a semi-spherical motion, as proposed in [46]. This approach ensures that the cells are positioned at the focal point of the lens; however, it does not guarantee that the cells rotate to align perpendicularly to the sun's rays, which can significantly reduce energy production.

$$\alpha_{max} = 90° - \phi + \delta_{max}, \tag{18}$$

$$\alpha_{min} = 90° - \phi - \delta_{max}. \tag{19}$$

Based on the analysis above, an optimized strategy was developed to minimize the displacement of CPV cells of the WiT-CPV throughout the year. The main idea is to install the WiT-CPV at a specific angle to ensure that the module is perpendicular to the sun's rays when the solar declination is 0° (see Fig. 7). First, the CPV module must be oriented southward in northern latitudes and northward in southern latitudes. Then, the optimal elevation angle (β_{opt}) of the module can be determined using Eq. (20). To achieve this elevation, the module must be tilted to the complementary angle of β_{opt}, which approximately corresponds to the latitude (ϕ). This approach is consistent with standard installation practices for conventional PV modules.

$$\beta_{opt} = \frac{\alpha_{max} + \alpha_{min}}{2}. \tag{20}$$

When the WiT-CPV is correctly oriented and tilted, a reference adjustment is applied. This adjustment ensures that the module remains perpendicular to the Sun's rays when the solar declination is 0°, which occurs during the autumnal and vernal equinoxes. By implementing this strategy, the system guarantees that the maximum solar deviation relative to the module along the zenith axis throughout the year will be ±23.5°, as it is precisely centered between the α_{max} and α_{min} values, as illustrated in Fig. 8.

Fig. 9 illustrates the spatial range that a CPV cell in a microtracking system can occupy at any latitude and date throughout the year, highlighted in orange. Fig. 9(a) depicts the space utilized by a microtracking system based on spherical guides [46], where the cell must traverse the entire hemisphere to remain aligned with the focal point of the lens. In contrast, Fig. 9(b) shows the path required for the CPV cells of the WiT-CPV at any latitude and date. Notably, the path is significantly reduced because the module is elevated to β_{opt}, limiting zenithal deviation to a maximum of ±23.5° in any latitude and date throughout the year. Considering that the optical efficiency of the CPV cell does not drop significantly at angles below 30° (see Fig. 6) and to keep the WiT-CPV system as simple as possible, the proposed design should track the lens's focal point throughout the year without rotating the CPV cell around the zenithal axis. This approach ensures that the CPV cell always remains parallel to the base of the concentrating lens. However, as previously mentioned, the cell must rotate along the azimuthal axis while simultaneously moving along the focal point of the lens.

Due to the wide acceptance angle, broad CPV cell movement range, and the prototype's tilt strategy, the system can position CPV cells along the solar trajectory for any latitude, accommodating varying solar radiation levels. This approach enhances operational efficiency, robustness, and sustainability. Furthermore, the proposed optimization of CPV cell movement in the WiT-CPV system reduces actuator energy consumption and mechanical wear, potentially extending their lifespan (to be explored in future research).

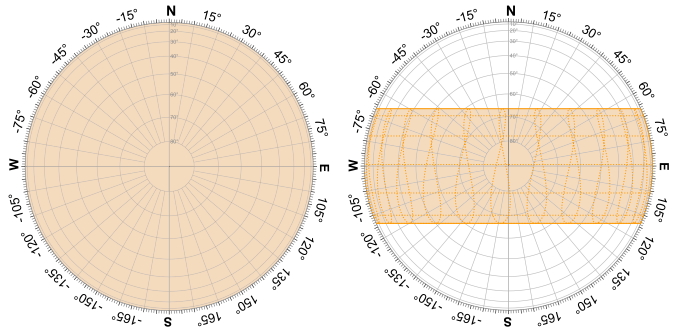


Fig. 9. Spatial range that a CPV cell in a microtracking system: a) system based on spherical guides and b) proposed WiT-CPV [55].

5.2. Mechanical design

The preceding analysis concludes that rotation along the zenith axis does not provide a favorable cost-benefit ratio. The minimal energy gains do not justify the increased complexity and cost of implementing zenithal rotation, so this adjustment has been excluded from the WiT-CPV design. This decision optimizes the balance between simplicity and performance, focusing on essential adjustments to maximize solar energy collection while minimizing mechanical complexity. The movement requirements for the CPV cells in the proposed WiT-CPV are summarized as follows:

A. Tracking the focal point along the zenithal axis: Continuous adjustment ensures optimal alignment with the sun's path throughout the year. This movement directly shifts the cells along the zenithal axis and indirectly along the Z-axis, moving them closer to or further away from the concentrating lens.
B. Tracking the focal point of the concentrating lens along the azimuthal axis ensures that the CPV cells remain aligned with the focal point's shifting position as the sun moves throughout the day. This movement directly shifts the cells along the azimuthal axis and indirectly along the Z-axis.
C. Rotation of the CPV cell in the azimuthal axis, centered on its midpoint: This adjustment allows the CPV cells to maintain a perpendicular orientation relative to the incident solar rays along the azimuthal plane, maximizing energy capture in this direction.

To achieve the abovementioned movements, a system was designed using linear actuators to transmit motion efficiently to the CPV cells. An XY table was implemented using three NEMA 11 linear modules with stepper motors and sliding stages: two modules with a 250 mm stroke for the azimuthal axis and one with a 150 mm stroke for the zenithal axis. No actuator was used for the Z-axis to further optimize the system and reduce the number of required actuators. Instead, acrylic guides were implemented to indirectly guide the cell's movement along this axis in response to adjustments made along the zenithal and azimuthal axes. This design enables precise control of the CPV cell positioning while minimizing mechanical complexity, cost, electrical consumption, and system maintenance. The system achieves high operational efficiency by streamlining these aspects without compromising performance. The following sections detail the drive mechanism for the azimuthal and zenithal axes.

5.2.1. Zenithal displacement mechanism

The zenith displacement mechanism is a critical component that enhances the system's alignment with solar movement by enabling precise adjustments to track the sun's zenith angle. This section describes the design and implementation of this mechanism, emphasizing its role in achieving fine-tuned positioning to optimize solar irradiance on the CPV cells throughout the year.

Fig. 10 illustrates the mechanism responsible for generating the zenith motion in the CPV cells of the WiT-CPV. The primary elements are color-coded for illustrative purposes. Four curved acrylic guides (black-colored) were implemented to ensure that the CPV cells move along the desired zenith axis path. A motion study conducted in SolidWorks was used to fine-tune the guide geometry, ensuring that the CPV cell center precisely follows the curvature of the concentrator lens's focal point along this axis. The guides were designed based on the trajectory described by Eq. (4), guaranteeing that any element constrained to slide along them will accurately track the focal point generated by the concentrating lens. Two round stainless steel tubes (pink-colored), each 3 mm in diameter, swing on these guides. These tubes are supported by four pieces (yellow-colored) attached to the bottom of Base 1. Two PET printed brackets (cyan-colored) transmit the movement of the two lateral linear zenithal actuators to Base 1 through the steel tubes. Although the brackets move linearly, Base 1 follows the precise curvature of the curved acrylic guides, enabling direct movement along the zenithal axis and indirect movement along the Z-axis. Notably, the CPV cells maintain a parallel movement relative to the lens at all times rather than rotating along the zenith axis. Furthermore, the movement of these cells along the zenith axis is characterized by its extremely slow pace, with a gradual shift from one extreme to the other occurring over the course of an entire year. This slow, parallel movement is a key design feature, as it significantly reduces energy consumption. Frequent adjustments along the zenith axis, which would be necessary with a more dynamic system, require higher energy expenditure due to the need to overcome gravitational forces. Therefore, this design choice directly translates to a highly energy-efficient system, which minimizes operational costs and maximizes the net energy output. However, if the module is not correctly oriented southward in northern latitudes or northward in southern latitudes, the system will operate with a slight adjustment to compensate for any deviation along this axis.

5.2.2. Azimuthal rotation and displacement mechanism

The WiT-CPV's azimuthal movement is similar to its zenithal movement. It utilizes a set of curved acrylic guides to ensure that the center of the CPV cell aligns with the focal point of the concentrator lens. However, since this axis requires the cell to rotate, the mechanism is slightly more complex. It primarily consists of three Bases, as illustrated in Fig. 11, with its operating principle described as follows:

- Base 1 is rigidly affixed to Base 3 by four spacer blocks (olive-colored), ensuring synchronized movement between the two bases.

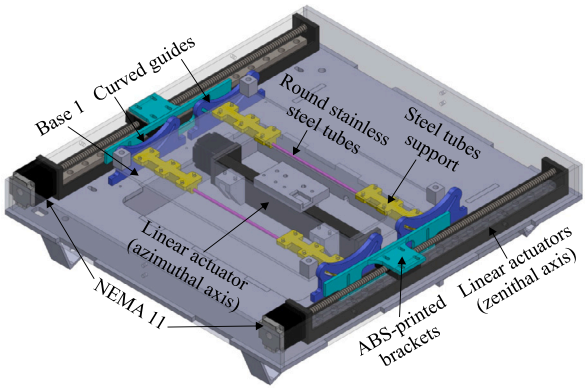


Fig. 10. Design of the zenithal displacement mechanism (the azimuth axis motion elements are hidden for better viewing).

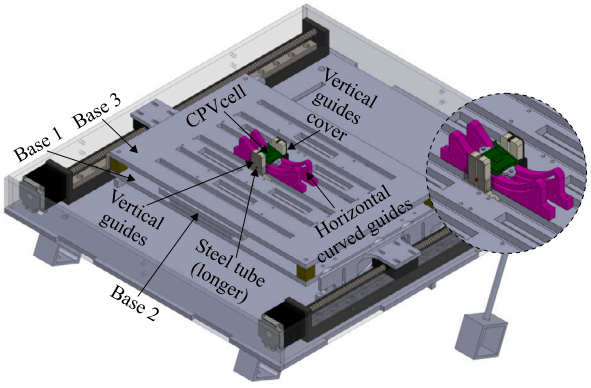


Fig. 11. Design of azimuthal displacement mechanism.

- Base 2 exhibits linear movement along the azimuthal axis. This motion is facilitated by the azimuthal linear actuator (see Fig. 10), mounted to the underside of Base 1, which provides support and enables Base 2 to translate smoothly between Bases 1 and 3. In addition, Base 2 features two vertical guides (beige-colored) per CPV cell. These guides transmit azimuthal motion via a 3 mm steel tube (red-colored) to a rail that supports the CPV cells.
- Base 3 incorporates two horizontal curved guides (fuchsia-colored) per CPV cell (green-colored), precisely engineered based on the trajectory described by Eq. (4) to maintain alignment between the cell center and the lens's focal point along the azimuthal axis. Each cell is mounted on these guides using a PET rail, which features three horizontal stainless steel tubes on its underside: a longer tube (red-colored tube) and two shorter tubes, as detailed in the inset of Fig. 11. The longer tube transmits the azimuthal movement by engaging with the vertical guide on Base 2, thereby accurately positioning the cell at the lens's focal point. The shorter tubes support the CPV cell rail, allowing it to rotate along the guide's curvature and maintain perpendicular alignment with incoming solar radiation throughout the day.

The above configuration converts the linear motion of the azimuthal actuators into a synchronized movement of the cell along both the azimuthal and Z axes. Furthermore, it enables automated cell rotation, maintaining perpendicular alignment between the cell and the lens's focal point and, consequently, with the incident solar radiation throughout the day. The system implements gradual azimuthal adjustments to maintain the cell's optimal orientation continuously. Notably, the cell's displacement and rotation are achieved through a single linear actuator, thereby minimizing electrical consumption and reducing system costs.

5.2.3. Mechanical design integration

Fig. 12 presents the complete design of the WiT-CPV system. As depicted, the tracking mechanism incorporates a control board compartment in its upper section. Additionally, the system incorporates four adjustable legs to enable precise module tilting at specific angles. An acrylic cover supports the array of concentration lenses. Only the central lens cell is considered for illustrative purposes in this prototype. For this image, the transparency of all acrylic materials was enabled to provide a clear visual demonstration of the system's design and functionality. It is important to mention that the WiT-CPV employs NEMA 11 stepper motor modules for their high torque, low cost, high precision, and low speed, essential for the prototype's precise movements. They maintain CPV cell positions without constant power, thereby enhancing efficiency and eliminating the need for encoders, which reduces complexity compared to DC motors. This supports scalability and suitability for agrivoltaic applications.

6. Controller board and control algorithm

The proposed controller board is designed considering that only the X and Y axes need to be controlled to track solar radiation fully, as the movement along the Z-axis of the module is mechanically obtained through the guides. Hence, two stepper drivers are incorporated, based on the TMC2209 controllers, which can achieve sensorless homing and low power consumption, crucial for increasing the energy obtained by the module. Fig. 13(a) illustrates the simplified block diagram of the proposed controller board, while Fig. 13(b) shows its PCB design. The proposed micro-controller unit (MCU) is based on an STM32L412KB, a Cortex-M4 MCU designed for low-power applications. To validate the tracking capabilities,

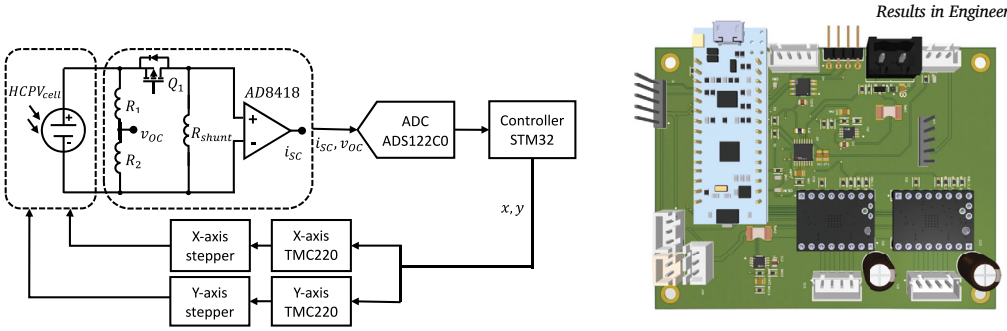


Fig. 12. Complete design of the WiT-CPV (rear isometric view).

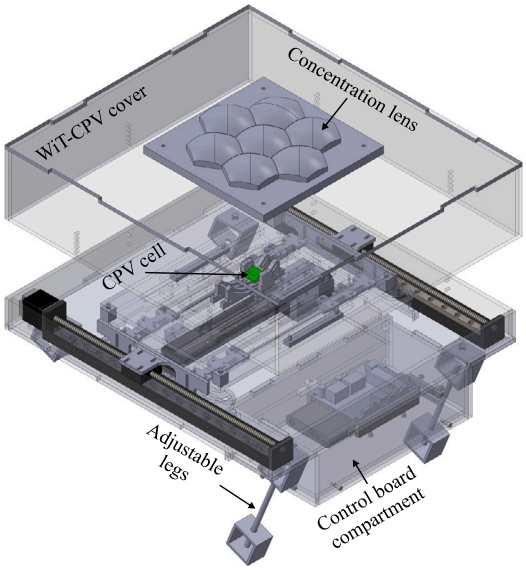


Fig. 13. Proposed controller board: (a) simplified block diagram and (b) PCB design.

the I_{sc}, is measured using a shunt resistor, an AD8418 current sense amplifier, and an ADS122C04 24-bit ADC to read the analog value and feed it to the MCU. Hence, the controller operates in a closed loop. Additionally, the open circuit voltage, V_{oc}, can also be measured by turning off the shunt resistor using transistor Q_1 and measuring the module's voltage through a voltage divider. An Apogee SP-212 pyranometer is integrated to measure the plane-of-array global irradiance, enabling future evaluation of the controller's effectiveness in tracking solar irradiation. The central control board performs data logging.

The MCU primarily utilizes the I_{sc} signal to monitor solar radiation. The control algorithm functions by comparing the I_{sc} value with the previous one, determining whether the system should continue in the same direction or reverse its movement. This process can be formulated as follows. For each axis, the difference between the current and previous I_{sc} values is calculated using Eq. (21), where $I_{sc,k}$ and $I_{sc,k-1}$ represent the I_{sc} signal values at the current and previous steps, respectively.

$$\Delta I_{sc,k} = I_{sc,k} - I_{sc,k-1}, \tag{21}$$

Based on the comparison, the direction of movement is determined by Eq. (22), where $d_k = 1$ indicates continued movement in the same direction, and $d_k = -1$ indicates a reversal.

$$d_k = \begin{cases} 1 & \text{if } \Delta I_{sc,k} > 0 \\ -1 & \text{if } \Delta I_{sc,k} < 0 \end{cases} \tag{22}$$

After determining the direction, the displacement at each iteration is adjusted progressively by Eq. (23),

$$\Delta x_k = \Delta x_{k-1} \cdot \left(1 - \frac{k}{N}\right), \tag{23}$$

where Δx_{k-1} is the displacement from the previous iteration, k is the current iteration step (ranging from 1 to 3), and N is the total number of iterations (3 in this case). The displacement decreases progressively with each iteration. This iterative process is applied to each axis, reducing displacement at each step to achieve efficient solar tracking. For clarity, the tracking procedure described above is summarized in Algorithm 1, which outlines the iterative control logic used to maximize I_{sc}. It is noteworthy that the results of solar irradiation tracking using the proposed device will be presented in a subsequent study.

Algorithm 1 Two-axis solar tracking algorithm based on solar cell I_{sc}.

for each axis **do**
  Initialize position $x \leftarrow x_0$
  Measure $I_{sc,0}$
  Set initial direction $d_0 \leftarrow 1$
  for $k = 1$ to N **do**
    Compute step size: $\Delta x_k \leftarrow \Delta x_{k-1} \cdot \left(1 - \frac{k}{N}\right)$
    Compute trial position: $x_k \leftarrow x + d_{k-1} \cdot \Delta x_k$
    Move to x_k and measure $I_{sc,k}$
    Compute $\Delta I_{sc,k} \leftarrow I_{sc,k} - I_{sc,k-1}$
    if $\Delta I_{sc,k} > 0$ **then**
      $x \leftarrow x_k$ ▷ Accept new position
      $d_k \leftarrow d_{k-1}$ ▷ Keep direction
    else
      $d_k \leftarrow -d_{k-1}$ ▷ Reverse direction for next iteration ▷ Keep current position x
    end if
  end for
end for

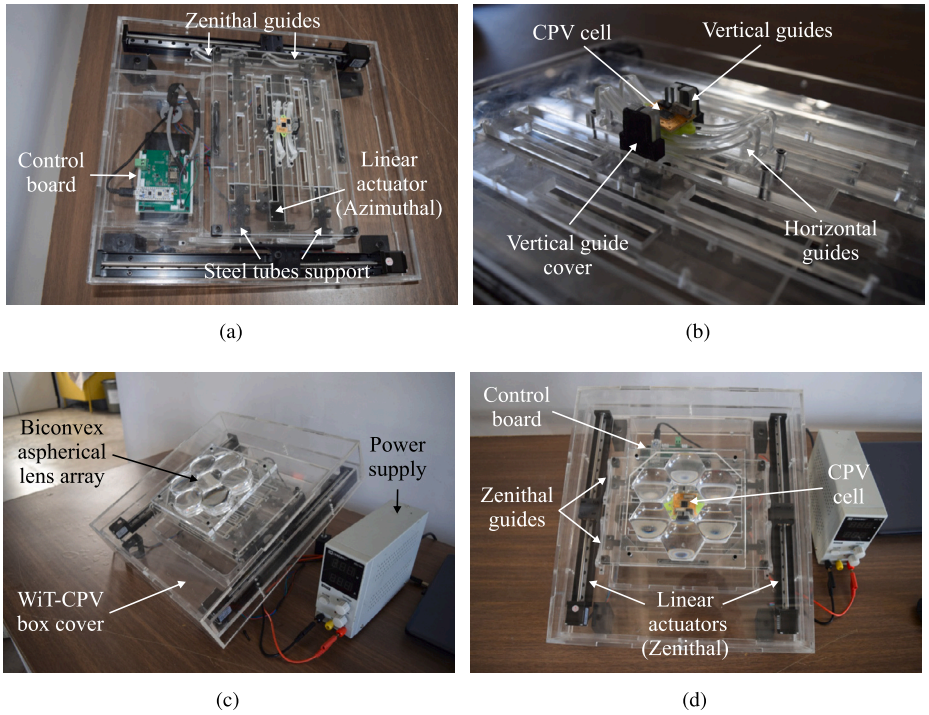


Fig. 14. WiT-CPV integration: a) guides for zenithal movement, b) guides for azimuthal movement, c) isometric view with focusing lenses, and d) top view with focusing lenses.

7. Results

7.1. WiT-CPV construction

Fig. 14 presents different perspectives of the fully constructed WiT-CPV prototype. As observed, all bases and the system's general cover were fabricated from 5 mm transparent acrylic. Consequently, radiation that is not incidental to the CPV cells passes through the module and reaches the surface below, facilitating its application in agrivoltaic systems. It is important to mention that the prototype was developed to validate the proof-of-concept under controlled laboratory conditions. Subsequent research will focus on conducting degradation and durability assessments to optimize material selection for enhanced long-term performance. It is also worth noting that the tracking algorithm implemented in the first version of the prototype (as described above) is straightforward and can be considered a starting point for testing the device under real sun conditions. The algorithm will be refined in future work to guarantee precise sun tracking even in varying irradiance conditions caused by clouds. Fig. 14(a) illustrates the main elements of the zenithal movement mechanism and the control board. Fig. 14(b) presents the primary elements of the azimuthal movement mechanism. Fig. 14(c) depicts an isometric view of the assembled WiT-CPV prototype and its power supply. Fig. 14(d) displays the frontal view of the WiT-CPV prototype, highlighting the CPV cell at the center of the concentration lens array. As observed, the majority of elements are fabricated from PET or 5 mm transparent acrylic, materials that are readily accessible and cost-effective. This choice contributes to a favorable cost-efficiency balance for the system. However, future versions will employ a material with enhanced durability against outdoor conditions, minimized degradation over time, and high optical transmittance.

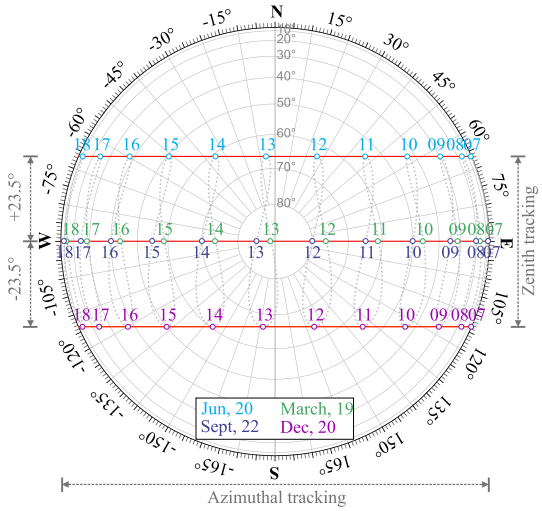


Fig. 15. Apparent solar path during different seasons for the WiT-CPV installed with the optimal tilt angle, southern orientation, and at the location of Aguascalientes, Mexico.

7.2. Experimental setup

The functionality of the WiT-CPV was validated through experimental tests. Initially, the optimal installation tilt angle for the WiT-CPV was calculated for Aguascalientes, Mexico, located at a latitude of 21.85° and longitude -102.33°. Using Eq. (20), the optimal elevation angle was determined to be $\beta_{opt} = 68.15°$. Consequently, the module was tilted to the complementary angle, 21.85°, which closely corresponds to the installation site's latitude. Then, the system was installed with a southerly orientation to optimize solar tracking. Subsequently, the zenithal and azimuthal movements were individually tested in open-loop (without feedback control) to ensure that the displacement range for each axis maintained the alignment of the cells with the focal point of the concentrator lens. It is noteworthy that once the CPV cells are positioned at the desired location along both axes, the actuators can be deactivated, eliminating power consumption and achieving minimal energy usage. The cells remain securely in position due to the system's transmission mechanism. Detailed validation of the movements for each axis is provided in the following sections.

7.3. Zenithal movement validation

As previously discussed, the apparent solar movement along the zenith axis progresses slowly throughout the year. Fig. 15 illustrates the apparent solar path during different seasons for the WiT-CPV installed with the optimal tilt angle ($\beta_{opt} = 68.15°$), southern orientation, and at the location of Aguascalientes, Mexico. As shown, the solar rays along the zenith axis exhibit a minimum incidence angle of −23.5° during the winter solstice (December 20) and a maximum incidence angle of +23.5° during the summer solstice (June 20). At the equinoxes (March 19 and September 22), the solar position is precisely perpendicular to the WiT-CPV on this axis. Consequently, the movement of the solar cells along the zenith axis changes gradually over the year, requiring minimal adjustments for alignment. Therefore, despite using two actuators for zenithal movement, they remain deactivated for extended periods because minimal daily adjustments are required.

For the above, the system must be capable of shifting the CPV cells by a minimum range equivalent to the focal point displacement of the concentrating lens, ±23.5°, to ensure adequate solar tracking for any date of the year and at any latitude. In this sense, a digital angle meter was used to measure the maximum displacement angle, confirming a range of up to ±30°, referenced to the normal of the proposed module. Hence, for the case study, the WiT-CPV can position the CPV cells within a range of 38.15° to 98.15°, fully covering the calculated values of $\alpha_{max} = 91.654817°$ and $\alpha_{min} = 44.654847°$ as determined by Eqs. (18) and (19), respectively. Video 1 (https://youtu.be/zMStF65mZI0, accessed on 13 March 2025) demonstrates the complete zenith axis movement. The mechanism's movement speed is adjustable through the control board, ensuring flexibility in response to solar movement.

7.4. Azimuthal movement validation

For the azimuthal axis, the WiT-CPV is designed to ensure that the CPV cells follow the lens focal point trajectory from east to west while maintaining a perpendicular alignment with the solar rays along this axis (see Fig. 15). The gradual east-to-west displacement of the cells throughout the day was verified. The movement of the CPV cells on the azimuthal axis is demonstrated in Video 2 (https://youtu.be/veD6nUGxIpQ, accessed on 13 March 2025). The cells' travel angle along this axis was measured using SolidWorks and a digital angle meter, showing a displacement range of ± 40°. This range allows the WiT-CPV to achieve a wide acceptance angle, enhancing its solar tracking capabilities. Additionally, the rotation of the cells along the azimuthal axis was verified. This configuration ensures the cells remain correctly perpendicular to the incident solar rays throughout the day. The system's movement accuracy and speed are configurable through the control program, allowing for fine-tuned operation to match specific solar tracking requirements.

The experimentation demonstrates that the proposed WiT-CPV, installed at the optimal tilt angle and oriented southward, requires nearly linear azimuthal movement of the CPV cells throughout the day. This minimizes zenith axis adjustments and significantly reduces energy consumption, confirming its efficiency and innovation in solar tracking technology.

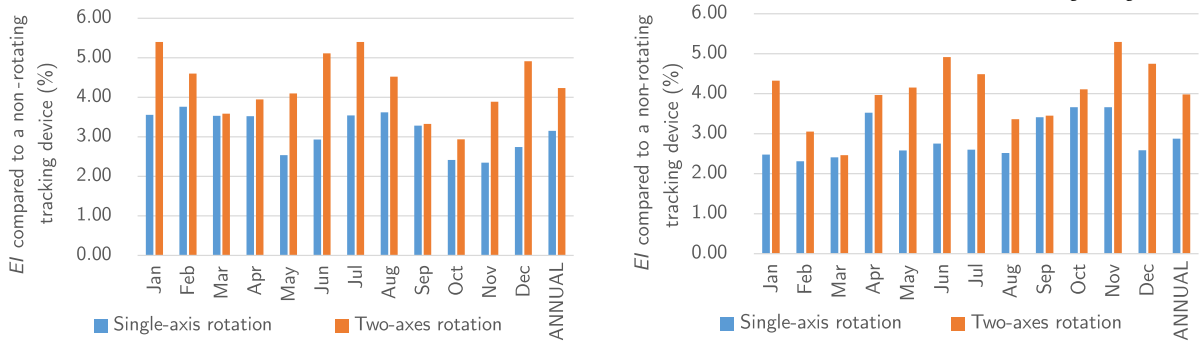


Fig. 16. Monthly and annual percentage energy improvement, EI (%), of single-axis and two-axis rotation devices compared to a non-rotating device in: a) Aguascalientes, Mexico, and b) Jaen, Spain.

7.5. Energy improvement analysis

An energy improvement analysis was performed to evaluate the performance of the proposed system. This analysis considered three configurations of microtracking mechanisms detailed in Section 4: (0) no rotation of the solar cell, (1) rotation along the azimuthal axis, and (2) full rotation of the solar cell along both the azimuthal and zenithal axes. The calculations were performed for two selected locations: Aguascalientes, Mexico (21.9° N, − 102.3°E) and Jaen, Spain (37.8° N, − 3.8°E). The latitudes of both sites differ significantly, allowing for a comparison of two locations with distinct solar paths and irradiance conditions. Both sites are characterized by elevated annual DNI values (Aguascalientes: 2,844 kWh/m^2; Jaen: 2,188 kWh/m^2). The meteorological data used to characterize these locations were obtained from the PVGIS software [56]. Specifically, the typical meteorological year files, which contain hourly values of the relevant parameters, were downloaded to perform the calculations.

Fig. 16(a) and Fig. 16(b) present the monthly and annual energy improvement (EI (%)) for Aguascalientes and Jaen, respectively. The results are shown for devices 1 (single-axis rotation) and 2 (two-axis rotation). As seen, the two-axis rotating device exhibits higher monthly and annual EI than the single-axis rotating device. This difference is greater during the summer and winter months, while it becomes minimal in March and September, coinciding with the equinoxes. Aguascalientes shows slightly higher EI values than Jaen, indicating that lowering the latitude enhances the benefits of rotating the solar cell. Regarding annual values, EI of 3.15% and 4.24% (single-axis and two-axis, respectively) are verified in Aguascalientes, while EI of 2.87% and 3.98% (single-axis and two-axis, respectively) are verified in Jaen. Therefore, compared to a non-rotating device, the single-axis rotation is a favorable option, as it provides appreciable energy gains (between 72% and 74% of the gains obtained by a two-axis rotating device) with a much simpler and cost-effective mechanical structure.

7.6. Comparative analysis of the WiT-CPV

At the current stage of the investigation, it is not possible to estimate the annual energy harvesting or energy yield of the developed microtracking system. This estimation will be part of future work. To get this estimation, the tracking algorithm will be refined and further validated, and an in-depth outdoor characterization that considers optical, spectral, and thermal effects will be developed. However, currently, it is possible to assess through simulations the annual energy gains of the developed prototype with azimuthal cell rotation compared to a similar system that does not rotate the cell. These gains are expected to be sufficient to justify the main innovation of the prototype, namely, the azimuthal rotation of the solar cell. Therefore, it was essential to assess through simulations the benefits of the azimuthal rotation compared to a non-rotating microtracking system.

As discussed earlier, the WiT-CPV system introduces a novel tracking mechanism that allows movement along the zenithal and azimuthal axes, optimizing solar alignment while maintaining mechanical simplicity. Along the zenithal axis, the CPV cell follows the focal point's trajectory without rotation, with a displacement range of ±30°, fully covering the focal movement range of ±23.5° (see Fig. 17(a)). The optical efficiency characterization confirms that the absence of cell rotation in this axis results in minimal losses, even at the maximum solar deviation of 23.5° (Fig. 6). In contrast, the azimuthal axis allows a displacement range of up to ±40°, providing greater flexibility in tracking the focal point across larger solar incidence angles (Fig. 17(b)). Unlike other micro-tracking CPV systems, the WiT-CPV incorporates azimuthal cell rotation, ensuring continuous perpendicularity to incoming rays. This capability significantly improves optical efficiency by reducing angular misalignment losses. Video 3 (https://youtu.be/NXAiq7LQYok, accessed March 13, 2025) showcases the coordinated movements of the WiT-CPV prototype, demonstrating its integrated micro-tracking functionality. The system also allows diffuse radiation to pass through the module, potentially benefiting dual-land-use applications such as agrivoltaics and greenhouse energy harvesting.

Although several studies have proposed integrated micro-tracking CPV systems, most lack detailed descriptions of prototype construction and do not incorporate cell rotation, as implemented in this work. Table 5 summarizes the key characteristics of these approaches. The majority relies on planar sliding mechanisms [43,41,42] or SMA actuators [44,45], both of which achieve only translational displacement without MJSC rotation. While some designs, such as [43], report exceptionally high peak optical efficiencies (> 95%), they lack mechanisms to maintain the solar cell perpendicular to incident rays, resulting in increased optical losses at mid-range incidence angles. Furthermore, SMA-based systems introduce challenges due to their nonlinear thermal behavior, reducing tracking accuracy under variable environmental conditions. In contrast, the WiT-CPV system is the first reported approach to integrate azimuthal rotation with full three-dimensional micro-tracking, requiring only three actuators. This novel mechanism maintains continuous perpendicular alignment with concentrated rays along the Petzval curve, minimizing optical losses across a wide range of incidence angles. Additionally, the optimized actuation strategy reduces power consumption by limiting the number of actuators, delivering a mechanically simple yet highly efficient tracking solution. By overcoming the limitations of SMA-based and purely translational designs, the WiT-CPV emerges as a competitive and scalable alternative for CPV tracking, significantly enhancing both optical performance and energy yield.

As seen in Table 5, few experimental micro-tracking CPV prototypes have been thoroughly characterized in the literature, and data regarding their optical performance remain scarce. The measured optical efficiency versus angle of incidence was reported for the prototype in [43], which

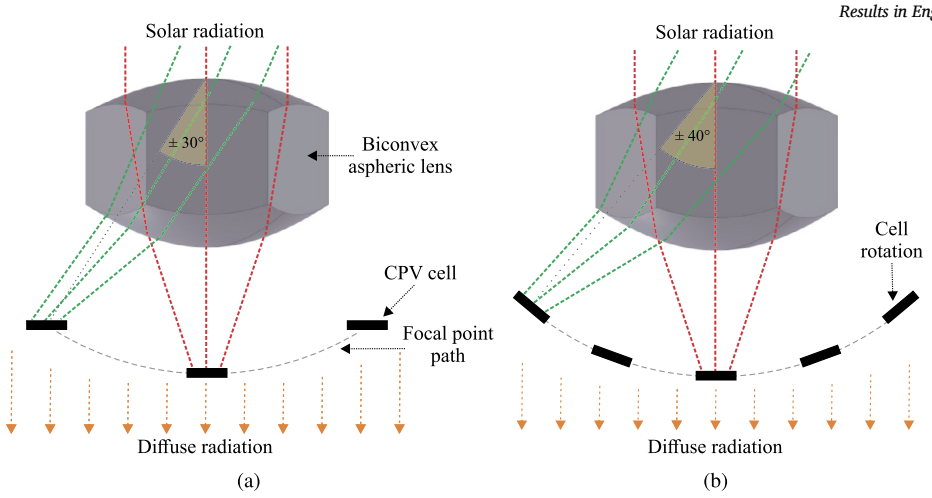


Fig. 17. Solar micro-tracking with the proposed WiT-CPV under different *AOI*: a) in the zenith axis (without cell rotation) and b) in the azimuth axis (with cell rotation).

Table 5
Comparison of different Integrated Micro-Tracking CPV Systems.

Ref.	Cell movement mechanism	*AOI*	η_{opt}	Concentr.	CR	N&T Actuators	Type
WiT-CPV (2025)	The solar cell movement is generated using three linear actuators: two for zenithal displacement (adjusting seasonally) and one for azimuthal tracking and cell rotation (changing daily). The zenithal actuators shift the cell along a curved guide, following the solar altitude, while the azimuthal actuator moves and rotates the cell to ensure perpendicular alignment with the incident sunlight.	±50°	> 80%	82.5×	Yes	Three stepper motors	Both
[40] (2024)	Solar cell moving across a flat surface, but no mechanism reported.	±40° (±70° at reduced efficiency)	78%	12.5×	No	NR	Sim
[57] (2023)	Solar cell plane translation via three-axis moving platform actuated by linear actuators (x–y lateral and z focus) inside the module.	±50°	82%	180×	No	Three linear actuators	Both
[10] (2023)	Manual movable triple-junction solar cell within a fixed bi-convex aspheric lens.	±50°	> 80% for 10× & > 60% for 82.5×	10× & 82.5×	No	NR	Both
[44] (2022)	Integrated tracking with SMA actuators (3D movement).	±35°	50 – 92%	> 200×	No	SMA wires	Both
[58] (2020)	Planar micro-tracking shifting backplane relative to optics and chassis.	±55°	~ 80%	180×	No	NR	Both
[41] (2018)	Lateral displacement of receiver over fixed mirror-coated lenslet array.	±45°	89.5%	50×	No	NR	Sim
[45] (2018)	Glass sheet with solar cells translating laterally, actuated by SMA wires.	NR	NR	NR	No	Three SMA wires	Exp
[46] (2018)	Three-dimensional micro-tracking with ball-foot guide.	±40°	~ 74%	127×	No	Two DC motors	Both
[59] (2018)	Magnetic technology for lateral movement of PV cells.	±60°	NR	180×	No	Magnetic actuator	Both
[43] (2017)	Integrated planar micro-tracking using lateral sliding of a glass sheet.	±70°	> 90%	660×	No	Two stepper motors	Both
[42] (2015)	Planar micro-tracking with photovoltaics between refractive and reflective lenslet arrays.	±55°	> 70%	> 200×	No	NR	Both

NR = not reported; Sim = simulation, Exp = experimental; Both = simulation and experimental; CR = cell rotation; N&T = Number and type.

employs a planar sliding mechanism with a glass sheet containing solar cells positioned between plano-convex refractive and reflective optics. While the reported peak optical efficiency of 97.3% surpasses that of the WiT-CPV (80.2%), comparing optical efficiency trends across different incidence angles reveals distinct advantages. Fig. 18 presents the normalized optical efficiency (i.e., the ratio of optical efficiency to its maximum value) as a function of the angle of incidence for both prototypes. Notably, the prototype in [43] exhibits an initial efficiency decay from 0° to 25°, whereas the WiT-CPV maintains a more stable optical response in this range. Between 25° and 40°, both systems exhibit a comparable linear decay, suggesting similar optical behavior. For higher incidence angles (40° to 50°), the Price et al. prototype performs better. However, since most solar energy is harvested within the low to mid-range angles (0° to 25°) in real-world applications, the WiT-CPV system provides a more stable optical efficiency profile, reinforcing its suitability for practical deployment.

7.7. Preliminary cost estimation of the WiT-CPV

A preliminary estimation of the cost per W_p that a CPV system built with WiT-CPV modules could achieve can be obtained by considering published standard costs. The global cost of a CPV system is expressed as [60]:

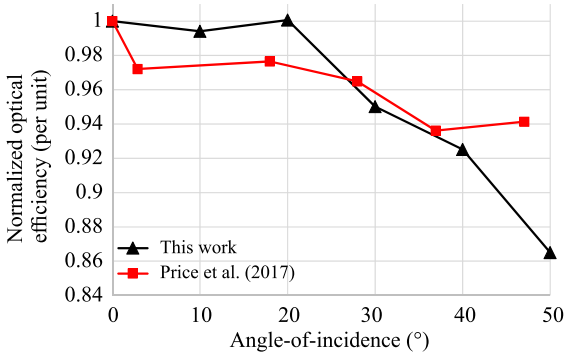


Fig. 18. Comparison of the normalized optical efficiency measured for the concentrator as a function of the angle of incidence.

$$\text{System cost } [€/W_p] = \frac{\dfrac{\text{Cell cost } [€/\text{m}^2]}{\text{Concentration}} + \text{Module cost } [€/\text{m}^2] + \text{Tracking cost } [€/\text{m}^2] + \text{BOS cost } [€/\text{m}^2]}{\text{Standard irradiance } [W/\text{m}^2] \cdot \text{System efficiency}} + \text{Inverter cost } [€/W_p]. \tag{24}$$

A multi-junction solar cell cost of 40 $/Wp was reported in [61], which, considering 40% solar cell efficiency and a current currency exchange rate of 1.16 $/€, corresponds to 13 793 €/m^2. The sum of module cost and tracking cost in conventional CPV systems is around 225 €/m^2 [60]. However, the solar tracker is removed in WiT-CPV, so this quantity can be reduced by about 130 €/m^2 (solar tracker cost as reported in [62]), resulting in 95 €/m^2. A BOS cost of 55 €/m^2 and an inverter cost of 0.11 €/Wp can also be considered according to [60], where the Balance of System (BOS) cost refers to all components and services of a photovoltaic system other than the solar cells and modules, including mounting structures, wiring, electrical protection, and installation labor. The concentration of WiT-CPV is 82.5×, and we can assume a system efficiency similar to that of conventional CPV systems, i.e., around 30% [63]. Therefore, with a standard irradiance of 1000 W/m^2, the estimated global cost of a WiT-CPV system could be around 1.17 €/Wp, which is comparable to standard fixed-structure crystalline silicon-based systems [64]. This means that a preliminary estimate of the WiT-CPV cost makes it competitive compared to standard PV technology. However, the proposed technology offers additional advantages, such as the possibility to be manufactured with transparent materials that allow diffuse light to pass through the modules, which can be valuable in agrivoltaic or building-integrated systems. It is worth highlighting that this cost estimation is preliminary and intended to assess the economic feasibility of the prototype. Further research and development are required to get a commercial product that verifies a cost level similar to that predicted.

8. Discussion

The WiT-CPV system demonstrates significant efficiency improvements through its innovative micro-tracking mechanism, as validated by simulation results (Section 7.5). By incorporating azimuthal cell rotation, the system achieves an annual energy increase of 3.15% and 2.87% compared to non-rotating configurations in Aguascalientes (2,844 kWh/m^2) and Jaén (2,188 kWh/m^2), respectively. The WiT-CPV system's adaptable design, with optimized tilt angles set to the installation site's latitude, ensures precise azimuthal alignment across a wide range and effective performance at any latitude, not limited to high-DNI zones. This configuration maintains stable optical efficiency at low-to-moderate angles (0°–25°, Fig. 18), supporting robust energy capture across diverse geographic locations while enabling effective performance despite varying irradiance levels. The mechanical complexity involved in implementing azimuthal rotation is higher than that of a non-rotating prototype. However, the developed system integrates cost-effective and easily manufacturable design enhancements. Therefore, the simulation of energy gains seeks to demonstrate that this prototype—while maintaining minimal mechanical complexity—can achieve significantly higher energy harvesting performance at an estimated system cost of 1.17 €/Wp, comparable to that of conventional crystalline silicon-based systems.

The WiT-CPV's scalability is enhanced by its modular architecture, utilizing only three linear actuators and acrylic guides. This design enables seamless expansion by adding guides to control multiple CPV arrays without the need for additional actuators, unlike most prototypes reported in the literature (see Table 5), which lack straightforward scalability. The WiT-CPV system's use of cost-effective materials (PMMA lenses, PET brackets) enhances economic viability, particularly for agrivoltaic applications where high land costs necessitate dual-land-use solutions. By transmitting diffuse radiation to support crop growth beneath the module, the system promotes sustainable farming in urban and rural settings, driving widespread adoption of agrivoltaic systems across diverse regions.

The WiT-CPV prototype, as a proof-of-concept, validates robust micro-tracking along zenithal (±30°) and azimuthal (±40°) axes, with azimuthal cell rotation ensuring perpendicular alignment to solar rays for enhanced energy capture. Unlike zenithal tracking, which omits cell rotation due to marginal gains, azimuthal rotation significantly reduces reflective losses, boosting optical efficiency. The current implementation uses transparent, non-final materials (e.g., acrylic) to demonstrate optical and mechanical viability in laboratory conditions, where long-term degradation and outdoor durability remain unassessed. Future iterations will incorporate durable, weather-resistant materials with high optical transmittance and require field trials to evaluate performance under temperature fluctuations, wind loads, and irradiance variations. Additionally, refining the tracking algorithm and conducting a detailed cost analysis, including the levelized cost of electricity (LCOE), will enhance scalability and commercial viability, particularly for agrivoltaic applications.

9. Conclusion

This study addressed CPV tracking challenges by developing and validating a proof-of-concept wide-acceptance-angle micro-concentrator photovoltaic system. The functional prototype, constructed from cost-effective materials such as PMMA and PET, integrated an innovative micro-tracking

mechanism with azimuthal cell rotation, enabling precise solar alignment with minimal mechanical complexity. Laboratory assembly and optical/mechanical characterization confirmed its performance, marking the first micro-tracking CPV prototype with azimuthal cell rotation. Key results include:

- Novelty: The WiT-CPV is the first reported micro-tracking prototype in the literature to incorporate azimuthal CPV cell rotation, ensuring perpendicular alignment with incident solar rays, significantly enhancing optical efficiency, and setting a new benchmark for micro-tracking CPV systems.
- Energy Gains: The WiT-CPV system demonstrated annual energy improvements of 3.15% in Aguascalientes, Mexico, and 2.87% in Jaén, Spain, compared to non-rotating systems, with single-axis rotation capturing 72–74% of dual-rotation tracking gains.
- Optical Performance: The prototype maintains stable optical efficiency at low incidence angles ($0° - 25°$), with performance comparable to top literature results at $25° - 40°$, ensuring effective energy capture.
- Mechanical Simplicity: The system employs three linear actuators and cost-effective materials (PMMA lenses, PET brackets) to achieve wide acceptance angles of $\pm 30°$ zenithal and $\pm 40°$ azimuthal, with azimuthal cell rotation ensuring perpendicular alignment with solar rays.
- Agrivoltaic Potential: The use of transparent materials enables diffuse radiation transmission, supporting dual-land-use applications like agrivoltaics.

Future work will involve integrating more durable materials, conducting outdoor field trials to evaluate long-term performance and material degradation, optimizing control algorithms for closed-loop operation and energy savings, performing extrusion tests with various polymers, and carrying out detailed cost analyzes, including the levelized cost of electricity (LCOE), to confirm commercial viability and techno-economic feasibility under real industrial conditions.

CRediT authorship contribution statement

Arturo Díaz-Ponce: Writing – original draft, Visualization, Methodology, Investigation, Conceptualization. **Iván Trejo-Zúñiga:** Writing – original draft, Validation, Formal analysis. **Fernando Dávalos Hernández:** Software, Investigation, Data curation. **Pedro M. Rodrigo:** Writing – original draft, Project administration, Investigation, Conceptualization. **María A. Ceballos:** Visualization, Resources, Formal analysis. **Álvaro Valera-Albacete:** Writing – original draft, Resources, Data curation. **Florencia Almonacid:** Writing – review & editing, Visualization, Investigation. **Eduardo F. Fernández:** Writing – review & editing, Supervision, Investigation.

Declaration of competing interest

The authors declare that they have no known competing financial interests or personal relationships that could have appeared to influence the work reported in this paper.

Acknowledgement

This work is part of the project WiT-CPV (grant CNS2022 – 135288), founded by MICIU/AEI/10.13039/501100011033 and the European Union. Additionally, the authors express their gratitude to Juan Margarito Sarabia Torres and Regina Montoya for their valuable contributions to the mechanical design and construction phases.

Data availability

No data was used for the research described in the article.

References

[1] M. Angulo-Calderón, I. Salgado-Tránsito, I. Trejo-Zúñiga, C. Paredes-Orta, S. Kesthkar, A. Díaz-Ponce, Development and accuracy assessment of a high-precision dual-axis pre-commercial solar tracker for concentrating photovoltaic modules, Appl. Sci. 12 (5) (2022) 2625, https://doi.org/10.3390/app12052625.
[2] H.A. Issa, L.M. Abdali, H. Alhusseini, V.I. Velkin, Design, modeling, and control of a dual-axis solar tracker using fractional order pid controllers for enhanced energy efficiency, Results Eng. 27 (2025) 106073, https://doi.org/10.1016/j.rineng.2025.106073.
[3] M. Fotopoulou, D. Rakopoulos, K.-N. Malamaki, N. Andriopoulos, G. Lampsidis, K. Kaousias, Photovoltaic penetration potential in the Greek island of ikaria, Sol. Compass 12 (2024) 100080, https://doi.org/10.1016/j.solcom.2024.100080.
[4] M.M. Abd-Elhady, M.A. Elhendawy, M.S. Abd-Elmajeed, R.B. Rizk, Enhancing photovoltaic systems: a comprehensive review of cooling, concentration, spectral splitting, and tracking techniques, Next Energy 6 (2025) 100185, https://doi.org/10.1016/j.nxener.2024.100185.
[5] C. Renno, Energy and economic comparison of three optical systems adopted in a point-focus CPV system, J. Braz. Soc. Mech. Sci. Eng. 44 (3) (Feb. 2022), https://doi.org/10.1007/s40430-022-03408-y.
[6] F.L. Rashid, M.A. Al-Obaidi, A.J. Mahdi, A. Ameen, Advancements in Fresnel lens technology across diverse solar energy applications: a comprehensive review, Energies 17 (3) (2024) 569, https://doi.org/10.3390/en17030569.
[7] Q.J. Abdul-Ghafoor, S.H. Abed, S.A. Kadhim, M.A. Al-Maliki, Experimental and numerical study of a linear Fresnel solar collector attached with dual axis tracking system, Results Eng. 23 (2024) 102543, https://doi.org/10.1016/j.rineng.2024.102543.
[8] R. Felsberger, A. Buchroithner, B. Gerl, B. Schweighofer, R. Preßmair, T. Mitter, H. Wegleiter, Optical performance and alignment characterization of a parabolic trough collector using a multi-junction CPV solar cell, Sol. Energy 239 (2022) 40–49, https://doi.org/10.1016/j.solener.2022.04.058.
[9] J.A. Dena, A. Díaz-Ponce, J.C. Delgado-Flores, E. Olvera-González, N. Escalante-García, V.M. Velasco-Gallardo, Design and construction of a solar electric plastic extruder machine based on a parabolic trough collector, IEEE Access 11 (2023) 124570–124583, https://doi.org/10.1109/access.2023.3328910.
[10] M.A. Ceballos, A. Valera, P. Sanmartín, F. Almonacid, E.F. Fernández, Development and indoor characterization of a concentrator photovoltaic assembly for tracking-integrated systems, Sol. Energy 255 (2023) 292–300, https://doi.org/10.1016/j.solener.2023.03.039.
[11] W. Iqbal, I. Ullah, S. Shin, Optical developments in concentrator photovoltaic systems—a review, Sustainability 15 (13) (2023) 10554, https://doi.org/10.3390/su151310554.
[12] S.P. Philipps, A.W. Bett, III-v multi-junction solar cells and concentrating photovoltaic (CPV) systems, Adv. Opt. Technol. 3 (5–6) (2014) 469–478, https://doi.org/10.1515/aot-2014-0051.
[13] A. Baiju, M. Yarema, Status and challenges of multi-junction solar cell technology, Front. Energy Res. 10 (Sep. 2022), https://doi.org/10.3389/fenrg.2022.971918.

[14] J.F. Geisz, R.M. France, K.L. Schulte, M.A. Steiner, A.G. Norman, H.L. Guthrey, M.R. Young, T. Song, T. Moriarty, Six-junction iii–v solar cells with 47.1% conversion efficiency under 143 suns concentration, Nat. Energy 5 (4) (2020) 326–335, https://doi.org/10.1038/s41560-020-0598-5.
[15] N.B. Desai, S. Bandyopadhyay, Line-focusing concentrating solar collector-based power plants: a review, Clean Technol. Environ. Policy 19 (1) (2016) 9–35, https://doi.org/10.1007/s10098-016-1238-4.
[16] S. Kannaiyan, N.D. Bokde, Z.W. Geem, Solar collectors modeling and controller design for solar thermal power plant, IEEE Access 8 (2020) 81425–81446, https://doi.org/10.1109/access.2020.2989003.
[17] T.Q. Saldivar-Aguilera, A. Diaz-Ponce, L.M. Valentin-Coronado, M.I. Pena-Cruz, G.A. Acevedo-R, Dual feedback closed-loop control for one-axis solar trackers of parabolic trough collector systems, in: 2021 IEEE International Autumn Meeting on Power, Electronics and Computing (ROPEC), IEEE, 2021, pp. 1–6.
[18] C. Xu, M. Li, X. Ji, F. Chen, Study on the collection efficiency of parabolic trough solar collector, in: 2013 International Conference on Materials for Renewable Energy and Environment, IEEE, 2013, pp. 1–7.
[19] H.A.K. Shahad, S.H. Hammad, N.A. Ghyadh, Design, fabrication and performance testing of ptc with helical coil receiver, in: 2019 4th Scientific International Conference Najaf (SICN), IEEE, 2019, pp. 189–194.
[20] K. Reddy, C. Ananthsornaraj, Design, development and performance investigation of solar parabolic trough collector for large-scale solar power plants, Renew. Energy 146 (2020) 1943–1957, https://doi.org/10.1016/j.renene.2019.07.158.
[21] V. Jebasingh, G.J. Herbert, A review of solar parabolic trough collector, Renew. Sustain. Energy Rev. 54 (2016) 1085–1091, https://doi.org/10.1016/j.rser.2015.10.043.
[22] B. Alhayek, M. Agelin-Chaab, B. Reddy, Analysis of an innovative direct steam generation-based parabolic trough collector plant hybridized with a biomass boiler, Int. J. Energy Res. 41 (14) (2017) 2236–2247, https://doi.org/10.1002/er.3785.
[23] S. Verma, S. Banerjee, R. Das, A fully analytical model of a box solar cooker with sensible thermal storage, Sol. Energy 233 (2022) 531–542, https://doi.org/10.1016/j.solener.2021.12.035.
[24] S. Verma, R. Das, Performance analysis of a solar still driven by a packed bed thermal storage tank during off-sunshine period, J. Energy Storage 44 (2021) 103381, https://doi.org/10.1016/j.est.2021.103381.
[25] G. Singh, R. Das, A novel variable refrigerant flow system with solar regeneration-based desiccant-assisted ventilation, Sol. Energy 238 (2022) 84–104, https://doi.org/10.1016/j.solener.2022.04.008.
[26] R.V. Parupudi, H. Singh, M. Kolokotroni, Low concentrating photovoltaics (LCPV) for buildings and their performance analyses, Appl. Energy 279 (2020) 115839, https://doi.org/10.1016/j.apenergy.2020.115839.
[27] S. Maestro, D. Chemisana, C. Lamnatou, Optics for smart building-integrated photovoltaic systems, Renew. Energy 246 (2025) 122850, https://doi.org/10.1016/j.renene.2025.122850.
[28] H. Coban, W. Lewicki, R. Miśkiewicz, W. Drożdż, The economic dimension of using the integration of highway sound screens with solar panels in the process of generating green energy, Energies 16 (1) (2022) 178, https://doi.org/10.3390/en16010178.
[29] S. Gorjian, F. Jalili Jamshidian, A. Gorjian, H. Faridi, M. Vafaei, F. Zhang, W. Liu, P. Elia Campana, Technological advancements and research prospects of innovative concentrating agrivoltaics, Appl. Energy 337 (2023) 120799, https://doi.org/10.1016/j.apenergy.2023.120799.
[30] T. Mallick, Challenges and opportunities in concentrating photovoltaic research, Mod. Energy Rev. 3 (2) (2011) 20–26.
[31] M. Wiesenfarth, I. Anton, A.W. Bett, Challenges in the design of concentrator photovoltaic (CPV) modules to achieve highest efficiencies, Appl. Phys. Rev. 5 (4) (Nov. 2018), https://doi.org/10.1063/1.5046752.
[32] R.F. Fuentes-Morales, A. Diaz-Ponce, M.I. Peña-Cruz, P.M. Rodrigo, L.M. Valentín-Coronado, F. Martell-Chavez, C.A. Pineda-Arellano, Control algorithms applied to active solar tracking systems: a review, Sol. Energy 212 (2020) 203–219, https://doi.org/10.1016/j.solener.2020.10.071.
[33] J. Canada-Bago, J.-A. Fernandez-Prieto, M.-A. Gadeo-Martos, P. Perez-Higueras, Knowledge-based sensors for controlling a high-concentration photovoltaic tracker, Sensors 20 (5) (2020) 1315, https://doi.org/10.3390/s20051315.
[34] A. Reinders, M. Wiesenfarth, R.R. King, Conceptual product development with integrated concentrating pv systems — CPV in the built environment from a designer's perspective, in: 2013 IEEE 39th Photovoltaic Specialists Conference (PVSC), IEEE, 2013, pp. 0474–0479.
[35] M.A. Ceballos, P.J. Pérez-Higueras, E.F. Fernández, F. Almonacid, Tracking-integrated CPV technology: state-of-the-art and classification, Energies 16 (15) (2023) 5605, https://doi.org/10.3390/en16155605.
[36] D.J. Wright, S. Badruddin, C. Robertson-Gillis, Micro-tracked CPV can be cost competitive with PV in behind-the-meter applications with demand charges, Front. Energy Res. 6 (Sep. 2018), https://doi.org/10.3389/fenrg.2018.00097.
[37] P. Kotsidas, E. Chatzi, V. Modi, Stationary nonimaging lenses for solar concentration, Appl. Opt. 49 (27) (2010) 5183, https://doi.org/10.1364/ao.49.005183.
[38] F. Duerr, P. Benítez, J.C. Miñano, Y. Meuret, H. Thienpont, Integrating tracking in concentrating photovoltaics using non-rotational symmetric laterally moving optics, in: R. Winston, J.M. Gordon (Eds.), in: Nonimaging Optics: Efficient Design for Illumination and Solar Concentration VIII, vol. 8124, SPIE, 2011, p. 81240M.
[39] F. Duerr, Y. Meuret, H. Thienpont, Tracking integration in concentrating photovoltaics using laterally moving optics, Opt. Express 19 (S3) (2011) A207, https://doi.org/10.1364/oe.19.00a207.
[40] S. Maestro, D. Chemisana, A. Moreno, Design and performance evaluation of a micro-CPV system for building integration applications, Sust. Energy Technol. Assess. 69 (2024) 103898, https://doi.org/10.1016/j.seta.2024.103898.
[41] N. Vu, S. Shin, Flat concentrator photovoltaic system with lateral displacement tracking for residential rooftops, Energies 11 (1) (2018) 114, https://doi.org/10.3390/en11010114.
[42] J.S. Price, X. Sheng, B.M. Meulblok, J.A. Rogers, N.C. Giebink, Wide-angle planar microtracking for quasi-static microcell concentrating photovoltaics, Nat. Commun. 6 (1) (Feb. 2015), https://doi.org/10.1038/ncomms7223.
[43] J.S. Price, A.J. Grede, B. Wang, M.V. Lipski, B. Fisher, K.-T. Lee, J. He, G.S. Brulo, X. Ma, S. Burroughs, C.D. Rahn, R.G. Nuzzo, J.A. Rogers, N.C. Giebink, High-concentration planar microtracking photovoltaic system exceeding 30% efficiency, Nat. Energy 2 (8) (Jul. 2017), https://doi.org/10.1038/nenergy.2017.113.
[44] A. Minuto, G. Timò, E. Celi, A New Cpv/Pv Hybrid Module with a Self-Powered, Integrated, 3d Meso Solar Tracker Based on Shape Memory Alloys, AIP Conference Proceedings, vol. 2550, AIP Publishing LLC, 2022, 060004.
[45] A.J. Grede, G.S. Brulo, A.J. Ren, M.D. Lenko, C.D. Rahn, N.C. Giebink, Motorless microtracking for rooftop cpv, in: 2018 IEEE 7th World Conference on Photovoltaic Energy Conversion (WCPEC) (a Joint Conference of 45th IEEE PVSC, 28th PVSEC & Amp; 34th EU PVSEC), 2018, pp. 1648–1651.
[46] A. Ito, D. Sato, N. Yamada, Optical design and demonstration of microtracking CPV module with bi-convex aspheric lens array, Opt. Express 26 (18) (2018) A879, https://doi.org/10.1364/oe.26.00a879.
[47] D.C. Miller, Analysis of transmitted optical spectrum enabling accelerated testing of multijunction concentrating photovoltaic designs, Opt. Eng. 50 (1) (2011) 013003, https://doi.org/10.1117/1.3530092.
[48] G. Beadie, M. Brindza, R.A. Flynn, A. Rosenberg, J.S. Shirk, Refractive index measurements of poly(methyl methacrylate) (pmma) from 04–16 μm, Appl. Opt. 54 (31) (2015) F139, https://doi.org/10.1364/ao.54.00f139.
[49] E.F. Fernández, A.J. García-Loureiro, G.P. Smestad, Multijunction concentrator solar cells: analysis and fundamentals, in: High Concentrator Photovoltaics: Fundamentals, Engineering and Power Plants, Springer, 2015, pp. 9–37.
[50] J.P. Ferrer-Rodríguez, H. Baig, E.F. Fernández, F. Almonacid, T. Mallick, P. Pérez-Higueras, Optical modeling of four Fresnel-based high-CPV units, Sol. Energy 155 (2017) 805–815, https://doi.org/10.1016/j.solener.2017.07.027.
[51] J.P. Ferrer-Rodríguez, E.F. Fernández, H. Baig, F. Almonacid, T. Mallick, P. Pérez, Higueras, development, indoor characterisation and comparison to optical modelling of four Fresnel-based high-CPV units equipped with refractive secondary optics, Sol. Energy Mater. Sol. Cells 186 (2018) 273–283, https://doi.org/10.1016/j.solmat.2018.06.050.
[52] International Organization for Standardization, ISO/TR 21900:2018 Guidance for uncertainty analysis regarding the application of ISO/TS 10974, Tech. Rep., ISO, 2018, https://www.iso.org/standard/72119.html. (Accessed 18 December 2024).
[53] J.A. Duffie, W.A. Beckman, Solar radiation, in: Solar Engineering of Thermal Processes, John Wiley & Sons, 2013, pp. 3–42.
[54] M. Iqbal, Chapter 1 - sun–Earth astronomical relationships, in: M. Iqbal (Ed.), An Introduction to Solar Radiation, Academic Press, 1983, pp. 1–28.
[55] A. Marsh, Sunpath 2d, https://drajmarsh.bitbucket.io/sunpath2d.html, 2023. (Accessed 5 November 2024).
[56] European Commission - EU Science Hub, Pvgis photovoltaic geographical information system, https://joint-research-centre.ec.europa.eu/pvgis-photovoltaic-geographical-information-system_en, 2024. (Accessed 26 May 2024).
[57] N. Jost, T. Gu, J. Hu, C. Domínguez, I. Antón, Integrated micro-scale concentrating photovoltaics: a scalable path toward high-efficiency, low-cost solar power, Solar RRL 7 (16) (Jul. 2023), https://doi.org/10.1002/solr.202300363.

[58] G. Nardin, C. Domínguez, Á.F. Aguilar, L. Anglade, M. Duchemin, D. Schuppisser, F. Gerlich, M. Ackermann, L. Coulot, B. Cuénod, et al., Industrialization of hybrid si/III–v and translucent planar micro-tracking modules, Progress in Photovolt. Res. Appl. 29 (7) (2020) 819–834, https://doi.org/10.1002/pip.3387.

[59] J. Lloyd, M. Pavilonis, C. Gladden, C. Casper, K. Schneider, W. McMahon, P. Kozodoy, Performance of a prototype stationary catadioptric concentrating photovoltaic module, Opt. Express 26 (10) (2018) A413, https://doi.org/10.1364/oe.26.00a413.

[60] N.J. Ekins-Daukes, P. Sandwell, J. Nelson, A.D. Johnson, G. Duggan, E. Herniak, What does CPV need to achieve in order to succeed?, AIP Conf. Proc. 1766 (2016) 020004, https://doi.org/10.1063/1.4962072.

[61] K.A.W. Horowitz, T. Remo, B. Smith, A. Ptak, A techno-economic analysis and cost reduction roadmap for III-V solar cells, Tech. Rep., National Renewable Energy Laboratory, 2018, https://docs.nrel.gov/docs/fy19osti/72103.pdf. (Accessed 3 August 2025).

[62] H. Apostoleris, M. Stefancich, M. Chiesa, Tracking-integrated systems for concentrating photovoltaics, Nat. Energy 1 (2016) 16018, https://doi.org/10.1038/nenergy.2016.18.

[63] P. Pérez-Higueras, J.P. Ferrer-Rodríguez, F. Almonacid, E.F. Fernández, Efficiency and acceptance angle of high concentrator photovoltaic modules: current status and indoor measurements, Renew. Sustain. Energy Rev. 94 (2018) 143–153.

[64] V. Ramasamy, J. Zuboy, M. Woodhouse, E. O'Shaughnessy, D. Feldman, J. Desai, et al., U.S. solar photovoltaic system and energy storage cost benchmarks, with minimum sustainable price analysis: Q1 2023, Tech. Rep., National Renewable Energy Laboratory, 2023, https://docs.nrel.gov/docs/fy23osti/87303.pdf. (Accessed 3 August 2025).